Review

The Reducing Agents in Sonochemical Reactions without Any Additives

Kyuichi Yasui

National Institute of Advanced Industrial Science and Technology (AIST), Nagoya 463-8560, Japan;
k.yasui@aist.go.jp

Abstract: It has been experimentally reported that not only oxidation reactions but also reduction reactions occur in aqueous solutions under ultrasound without any additives. According to the numerical simulations of chemical reactions inside an air or argon bubble in water without any additives under ultrasound, reducing agents produced from the bubbles are H, H_2, HO_2 (which becomes superoxide anion (O_2^-) in liquid water), NO, and HNO_2 (which becomes NO_2^- in liquid water). In addition, H_2O_2 sometimes works as a reducing agent. As the reduction potentials of H and H_2 (in strongly alkaline solutions for H_2) are higher than those of RCHOH radicals, which are usually used to reduce metal ions, H and H_2 generated from cavitation bubbles are expected to reduce metal ions to produce metal nanoparticles (in strongly alkaline solutions for H_2 to work). It is possible that the superoxide anion (O_2^-) also plays some role in the sonochemical reduction of some solutes. In strongly alkaline solutions, hydrated electrons ($e^-(aq)$) formed from H atoms in liquid water may play an important role in the sonochemical reduction of solutes because the reduction potential is extremely high. The influence of ultrasonic frequency on the amount of H atoms produced from a cavitation bubble is also discussed.

Keywords: sonochemistry; reducing agents; an air or argon bubble; ultrasound; numerical simulations; bubble collapse; chemical reactions; water vapor; H atoms
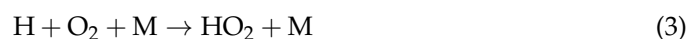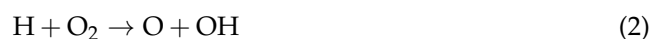
1. Introduction

An ultrasonic bath is widely used for cleaning glass, medical equipment, etc. [1,2]. Furthermore, an ultrasonic bath is widely used in laboratories for the dispersion of nanoparticles in various liquids [3–6]. An ultrasonic horn is also widely used in the dispersion of nanoparticles as well as in the dissolution of gels [3–11]. The physical and chemical effects of strong ultrasound are mostly caused by acoustic cavitation, which is the formation of gas bubbles and the violent collapse of the bubbles under ultrasound [2]. When the acoustic pressure amplitude is larger than the cavitation threshold, many tiny bubbles of a few micrometers in diameter are created [2,12–16]. During the rarefaction phase of ultrasound, the bubbles expand. At the compression phase of ultrasound, some of the bubbles violently collapse, which is called the Rayleigh collapse [2,17,18]. The reasons for the violent bubble collapse are as follows [2,18]. One is the inertia of the inflowing liquid toward the bubble during the bubble collapse. The other is the nearly spherical geometry of the bubble collapse, as the continuity of the liquid requires an increase in the inward liquid velocity as the distance from the bubble center decreases because the surface area decreases. The violent collapse stops when the gas density inside the bubble increases nearly to the density of liquid (the condensed phase) because the internal pressure of the bubble significantly increases [2,19]. At the final moment of the violent bubble collapse, the temperature and pressure inside the bubble increase to several thousand Kelvin and several hundred of atmospheric pressure or more because the work performed on a collapsing bubble by the surrounding liquid heats up the bubble [2,12,19–22]. In other words, it is a quasi-adiabatic collapse, where "quasi-" means that appreciable thermal conduction takes place between the heated interior of a

bubble and the surrounding liquid [12]. As a result, water vapor and oxygen, if present, are thermally dissociated inside a heated bubble, and oxidants such as OH radicals, H_2O_2, and O radicals are formed [2,23–25]. In addition, faint light is emitted from the heated bubbles, which is called sonoluminescence, partly because gases inside heated bubbles are weakly ionized [2,12,17,20,26–32]. The oxidants diffuse into the liquid and react with solutes, which are called sonochemical reactions [2,23,33–39]. Sonochemical reactions in aqueous solutions are mostly the oxidation of solutes, as easily confirmed by the chemiluminescence of luminol, which is called sonochemiluminescence [2,23,40–50]. The oxidation of potassium iodide (Reaction (1)) is widely used as a dosimeter to calibrate sonochemical efficiency [2,51,52].

$$2OH + 3I^- \rightarrow 2OH^- + I_3^- \tag{1}$$

The chemical products from cavitation bubbles under ultrasound are mostly oxidants because H atoms, which are reducing agents, formed inside a bubble by the dissociation of water vapor hardly penetrate into the liquid phase due to the chemical reactions with O_2 and OH inside a bubble as follows [53].

$$H + O_2 \rightarrow O + OH \tag{2}$$

$$H + O_2 + M \rightarrow HO_2 + M \tag{3}$$

$$H + OH \rightarrow H_2 + O \tag{4}$$

On the other hand, the sonochemical reduction of metal ions to produce metal nanoparticles has been experimentally reported [54–73]. In most of the experiments, an organic material such as alcohol (RCH_2OH, where R = H or alkyl group), ascorbic acid, formic acid, etc., was added to the aqueous solution to produce a reducing agent by the chemical reaction with OH radicals generated from cavitation bubbles as follows for alcohol [54–61,65,66,68,71–73].

$$RCH_2OH + OH \rightarrow RCHOH + H_2O \tag{5}$$
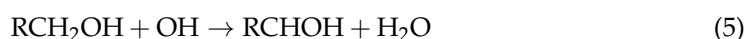
where RCHOH is a reducing agent (radical) and reduces metal ions as follows [57,61,68].

$$3RCHOH + AuCl_4^- \rightarrow 3RCHO + 3H^+ + Au + 4Cl^- \tag{6}$$
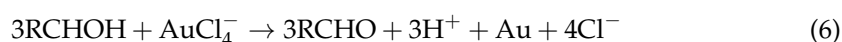
Citric acid and EDTA also produce reducing agents by reacting with OH radicals [74,75].
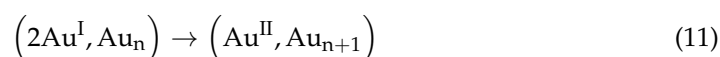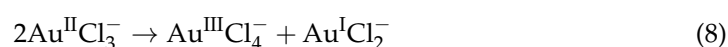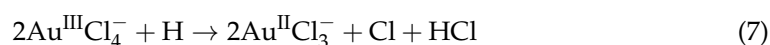
In 2020, Okitsu et al. [76] reported that in the experiment of sonochemical reduction of $AuCl_4^-$ in aqueous butanol ($CH_3(CH_2)_3OH$) solution under Ar at 200 kHz, the main reducing agents were CO, CH_3, and other products of pyrolysis of butanol by acoustic cavitation. It has been known that volatile solutes such as low-molecular-weight alcohols enter cavitation bubbles and are dissociated in the heated bubbles at the violent bubble collapse [2,77]. Kamali et al. [78] suggested that zero-valent copper was formed by the thermal decomposition of copper (II) acetate monohydrate ($Cu(CO_2CH_3)_2 \cdot H_2O$) inside heated cavitation bubbles at the violent bubble collapse. However, in their experiment [78], an ethylene glycol-ethanol solution (1:1) was used, and reducing agents might be formed by the thermal decomposition of ethylene glycol and/or ethanol. Further studies are required on this topic.

On the other hand, there are a few experimental reports that metal ions are reduced in sonochemical reactions without any additives such as organic materials, as discussed in more detail in the following section [68–70]. In the present review, reducing agents in sonochemical reactions without any additives are discussed based on numerical simulations of chemical reactions inside an air or argon bubble [24,53]. One of the aims of the present review is to stress that not only oxidation reactions but also reduction reactions occur in sonochemical reactions without any additives. Another aim is to discuss the chall-enges faced in this field and the outlook for research direction. The other aim is to

provide information to enhance the reduction reactions in sonochemical reactions without adding any additives.

2. Sonochemical Reduction without Any Additives

In 2009, Sakai et al. [69] experimentally reported the sonochemical reduction of $AuCl_4^-$ ions in an aqueous $HAuCl_4$ solution in the concentration range of 0.01–0.1 mM without any additives. The solution was irradiated with ultrasound in an ultrasonic bath, which enabled it to generate 28, 200, and 950 kHz ultrasound. The liquid temperature ranged from 4 to 60 °C. Ultra-pure water used in the experiment was purged by argon gas to promote radical (H and OH) formation from water. The proposed chemical reactions in the solution under ultrasound are as follows [69].

$$2Au^{III}Cl_4^- + H \rightarrow 2Au^{II}Cl_3^- + Cl + HCl \tag{7}$$

$$2Au^{II}Cl_3^- \rightarrow Au^{III}Cl_4^- + Au^{I}Cl_2^- \tag{8}$$

$$Au^{I}Cl_2^- + H \rightarrow Au^0 + HCl + Cl^- \tag{9}$$

$$nAu^0 \rightarrow \left(Au^0\right)_n \tag{10}$$

$$\left(2Au^I, Au_n\right) \rightarrow \left(Au^{II}, Au_{n+1}\right) \tag{11}$$

$$Au^{III}Cl_4^- + 2Au^0 + 2Cl^- \leftrightarrow 3Au^{I}Cl_2^- \tag{12}$$

In the experiment of Sakai et al. [69], the reduction of $AuCl_4^-$ was monitored by the decrease of the $AuCl_4^-$ concentration ($\left[Au^{III}\right]$) in solutions with an inductively coupled plasma spectrometer (ICPS) (ICPS-7500, SHIMADZU, Kyoto, Japan). The formation of gold nanoparticles was confirmed by observing the absorption spectra at ~530 nm originating from the surface plasmon resonance of the gold nanoparticles using a UV-visible spectrometer. The size and shape of the produced gold nanoparticles were observed by transmission electron microscopy (TEM) (H-7650, Hitachi High Technologies Co., Tokyo, Japan).

Experimental evidence for the sonochemical reduction of $AuCl_4^-$ without any additive is the decrease of $AuCl_4^-$ concentration with time measured with ICPS, as shown in Figure 1 [69]. The concentration of $AuCl_4^-$ ions in the solution decreased with sonication time and became zero at ~6 min in the case of 200 and 950 kHz sonication (Figure 1). In the case of 28 kHz sonication, the decrease in $AuCl_4^-$ concentration was not significant. They indicate that higher-frequency ultrasound is more effective at reducing $AuCl_4^-$ than lower-frequency ultrasound. In the case of 200 and 950 kHz sonication, an absorption band centered at ~530 nm originated from the surface plasmon resonance of the gold nanoparticles was observed using a UV-visible spectrometer [69]. In the case of 28 kHz, there was no noticeable peak in the absorption spectrum. The facts also indicate that appreciable amounts of gold nanoparticles were produced for the cases of 200 and 950 kHz sonication, while much less gold nanoparticles were produced for the case of 28 kHz sonication.

According to the TEM observation of the produced gold nanoparticles formed from aqueous 0.1 mM $AuCl_4^-$ solutions by 950 kHz sonication for 8 min, there were spherical nanoparticles with a diameter of 20–60 nm and triangular and/or hexagonal plates with a size of 20–200 nm, as shown in Figure 2 [69]. As seen in Figure 2, the size and shape of the produced gold nanoparticles depend on the liquid temperature during the sonication. For the temperature range of 4–40 °C, triangular and hexagonal plates were formed along with the spherical nanoparticles. On the other hand, for the cases of 50 and 60 °C, only spherical gold nanoparticles were formed, as shown in Figure 2 [69]. Sakai et al. [69] suggested that under relatively high liquid temperatures, dissolution of triangular and hexagonal plates would be accelerated because, 30 days after the preparation of gold nanoparticles at 25 °C, triangular and hexagonal plates disappeared. With regard to the mechanism for

the formation of triangular and hexagonal plates, Sakai et al. [69,70] suggested that Cl^- ions are adsorbed on a certain crystal facet and reduction of $AuCl_4^-$ ions occurs on other crystal facets. Indeed, the formation of triangular and/or hexagonal plates was promoted with the addition of NaCl, and the size of the plate increased as the NaCl concentration increased [69]. The larger size of triangular and hexagonal plates compared to spherical nanoparticles may be due to the accelerated reduction of $AuCl_4^-$ ions on the crystal facets of the plates. Further studies are required on this topic.
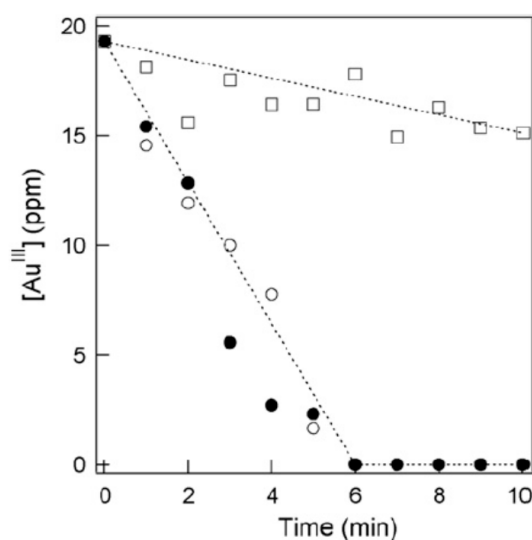
Figure 1. The concentration of $AuCl_4^-$ ($[Au^{III}]$) as a function of sonication time, using different frequencies of ultrasound: 28 kHz (□), 200 kHz (○), and 950 kHz (●) at 25 °C. The initial concentration of $AuCl_4^-$ was 0.1 mM. Reprinted with permission from Ref. [69]. Copyright 2009, Elsevier.

In 2014, Sakai et al. [70] experimentally reported the influence of gas species on the sonochemical reduction of $AuCl_4^-$ without any additives (Figures 3 and 4). The gas species studied were Ar, N_2, O_2, and H_2. Aqueous 0.1 mM $AuCl_4^-$ solutions were purged with each gas for 30 min before sonication [70]. The solutions were sonicated in an ultrasonic bath at 950 kHz for 8 min at 25 °C [70]. For an Ar-purged solution, spherical and plate-like gold nanoparticles were produced (Figure 3a). Indeed, bimodal absorption bands centered at ~520 and ~720 nm originated from the surface plasmon resonance of the spherical and plate-like gold nanoparticles, respectively, were observed (Figure 4a). For a N_2-purged solution, the gold nanoparticles produced were similar to those for the Ar-purged solution (Figure 3b). However, the size of plate-like gold nanoparticles produced from the N_2-purged solution seems to be larger than those from the Ar-purged solution because the absorption band was shifted to a longer wavelength (Figure 4b) [70,79]. For an O_2-purged solution, larger gold nanoparticles were produced compared to those for the Ar-purged and N_2-purged solutions (Figures 3c and 4c) [70]. On the other hand, for a H_2-purged solution, spherical gold nanoparticles of ~20 nm were selectively produced (Figures 3d and 4d) [70]. It should be noted that gas purging alone without sonication did not reduce $AuCl_4^-$ in aqueous solutions [70]. Sakai et al. [70] suggested that the formation of smaller spherical gold nanoparticles in the H_2-purged solution is due to the increase in the number of nanoparticle nucleation sites caused by the increase in the amount of the reducing agent (H atoms) by the following reaction.

$$OH + H_2 \rightarrow H_2O + H \tag{13}$$

where OH radicals are produced by the thermal dissociation of water vapor in the heated hydrogen bubbles at the violent bubble collapse [80,81]. Although Sakai et al. [70] did not comment on the site where the reaction (13) occurs, it seems that the reaction (13) occurs at the gas-liquid interface region shown in Figure 5 [82]. Sakai et al. [70] discussed that the

reducing agent (H atoms) produced inside oxygen bubbles from water vapor at the violent bubble collapse is consumed by the following reaction in an O_2-purged solution.

$$H + O_2 \rightarrow HO_2 \tag{14}$$

Indeed, according to the numerical simulations of chemical reactions inside an oxygen (O_2) bubble in water irradiated by 22 kHz and 1.68 bar ultrasound [83], the main chemical products are H and HO_2, along with H_2, H_2O_2, and OH radicals. It seems that H atoms are consumed in the gas-liquid interface region by the reaction (14). Accordingly, the number of nanoparticle nucleation sites is decreased in an O_2-purged solution, and the particle size is increased due to the smaller number of particles generated. Although Sakai et al. [70] also discussed the reason for the similarity in gold nanoparticle production in Ar-purged and N_2-purged solutions, it seems to be unclear at present.
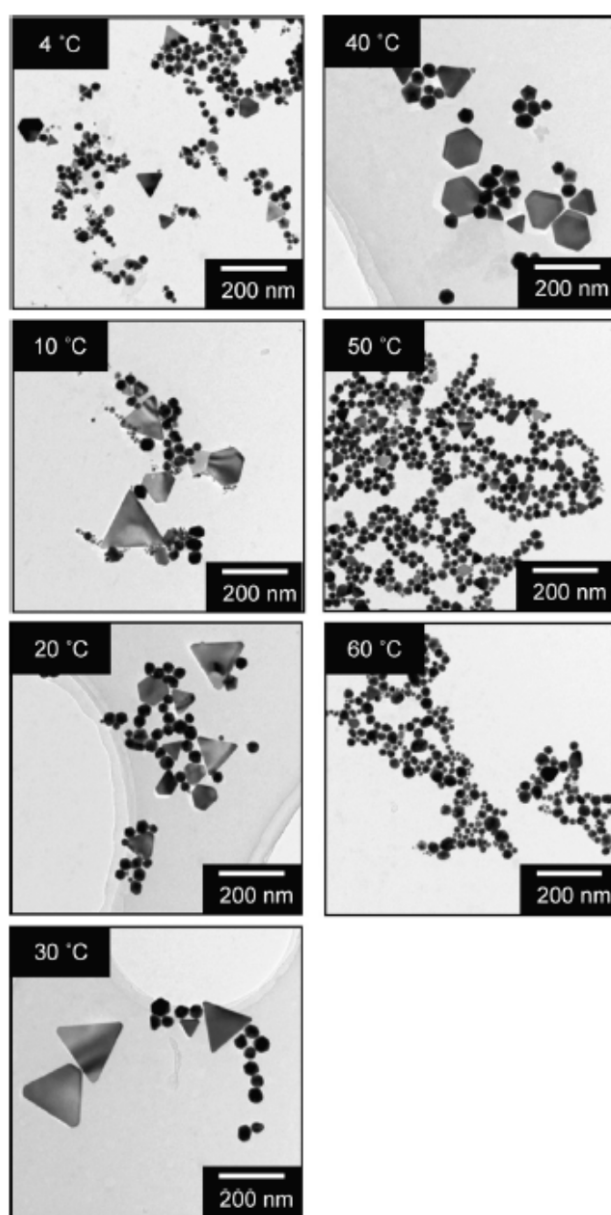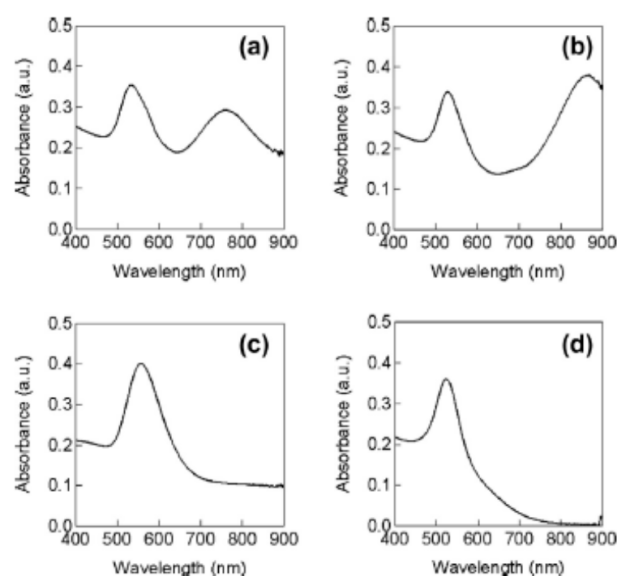

Figure 2. TEM images of gold nanoparticles formed from aqueous 0.1 mM $AuCl_4^-$ solutions by 950 kHz sonication for 8 min at 4, 10, 20, 30, 40, 50, and 60 °C. Reprinted with permission from Ref. [69]. Copyright 2009, Elsevier.
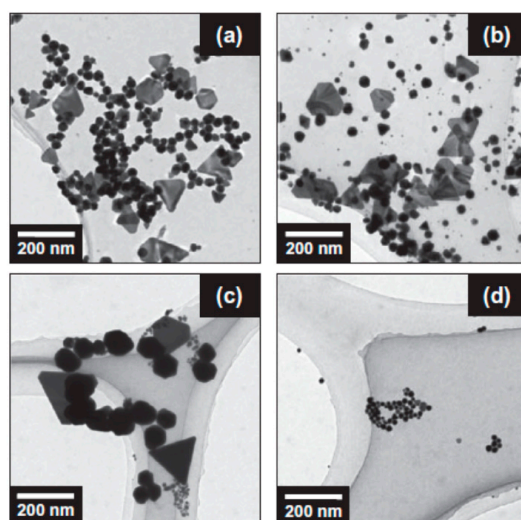
Figure 3. TEM images of gold nanoparticles formed from (**a**) Ar-, (**b**) N$_2$-, (**c**) O$_2$-, and (**d**) H$_2$-purged aqueous 0.1 mM AuCl$_4^-$ solutions by 950 kHz sonication for 8 min at 25 °C. The solutions were purged with gas for 30 min. Reprinted with permission from Ref. [70]. Copyright 2014, Elsevier.

Figure 4. Absorption spectra originating from surface plasmon resonance of gold nanoparticles formed from (**a**) Ar-, (**b**) N$_2$-, (**c**) O$_2$-, and (**d**) H$_2$-purged aqueous 0.1 mM AuCl$_4^-$ solutions by 950 kHz sonication for 8 min at 25 °C. Reprinted with permission from Ref. [70]. Copyright 2014, Elsevier.
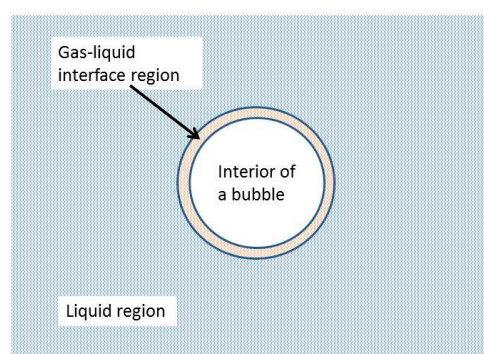

Figure 5. Three regions for a cavitation bubble. Reprinted with permission from Ref. [82]. Copyright 2016, Springer Nature.

In 2020, Yasuda et al. [84] experimentally reported the sonochemical reduction of $AuCl_4^-$ without any additives such as organic materials with and without ultrafine bubbles (UFBs, which are also called bulk nanobubbles). In the experiment [84], UFBs were generated by a pressurized dissolution method using ultrapure water and a commercially available UFB generator. Air, argon, oxygen, and nitrogen were used as gases to generate UFBs [84]. During the generation of UFBs, the liquid becomes milky due to the generation of a huge number of microbubbles, mostly using hydrodynamic cavitation [85,86]. After stopping cavitation, the liquid returns to being transparent as most of the microbubbles disappear at the liquid surface due to buoyancy. In the transparent liquid water, UFBs are present, which can be confirmed by particle tracking analysis (PTA) to estimate the number concentration and size distribution of nano and submicron particles suspended in a liquid by observing the Brownian motion of the particles with a video camera [85,87]. The size distribution of micro and ultrafine bubbles in the initial milky water is continuous, and only ultrafine bubbles of about 100 nm in diameter remain in the transparent liquid [87,88]. In the experiment of Yasuda et al. [84], the modal diameters of UFBs for all the gases were approximately 120 nm. The concentration of air-UFBs before ultrasonic irradiation was 5×10^9 mL^{-1} [84]. It should be noted that UFBs are generally very stable, and the lifetime could be more than 200 days with a slight change in size distribution [88,89]. With regard to the mechanism of stability of a UFB against dissolution, the dynamic equilibrium model that a UFB is partly covered with hydrophobic materials (impurities) seems promising because there is evidence in the TEM images of UFBs partly covered with hydrophobic materials [90–96]. In the experiment of Yasuda et al. [84], water containing UFBs was used as solvent for aqueous 0.1 mM $AuCl_4^-$ solutions. The solution was irradiated with 495 kHz ultrasound using the apparatus shown in Figure 6i [84]. As is usually the case in experiments in sonochemistry [2,97], a sinusoidal electric signal is amplified with a power amplifier and supplied to an ultrasonic transducer, which is attached to the bottom of an ultrasonic bath. A vessel that contained the solution was immersed in the ultrasonic bath filled with water, as shown in Figure 6i. The comparison between sonochemically produced gold nanoparticles with and without air-UFBs is shown in Figure 6ii,iii. Without UFBs, the produced gold nanoparticles were not only spherical nanoparticles but also plate-like particles (Figure 6ii(a)). The mean diameter of the particles without UFBs was 119 nm [84]. On the other hand, with air-UFBs, mostly spherical gold nanoparticles were produced. Furthermore, the gold nanoparticles produced were much smaller than those without UFBs. The mean diameter of gold nanoparticles with air-UFBs was 22 nm [84]. This is confirmed by the absorption spectra because the absorption peak became sharper and was shifted to a shorter wavelength with air-UFBs compared to that without UFBs (Figure 6iii) [79,84]. For all the gases for UFBs studied by Yasuda et al. [84], the produced gold nanoparticles were mostly spherical nanoparticles, in contrast to the case without UFBs. The mean diameter of the produced gold nanoparticles depended on the gas species: 49 nm for Ar-UFBs, 43 nm for O_2-UFBs, 73 nm for N_2-UFBs, and 22 nm for air-UFBs [84]. Yasuda et al. [84] suggested that acoustic cavitation could be enhanced in the presence of UFBs, and accordingly, the concentration of reducing species could be increased. It may result in an increase in nucleation sites in nanoparticles and a decrease in particle size [84]. On the other hand, according to the dynamic equilibrium model of UFBs [90], a UFB is stabilized against dissolution by being partly covered with hydrophobic impurities such as oils, carbon particles, etc. The hydrophobic impurities could be produced from a UFB generator, such as abrasion powder from the mechanical seal or lubrication oil in a water pump, even if ultrapure water is used [98,99]. It suggests that sonication of the hydrophobic impurities may result in the production of reducing agents such as CO, CH_3, etc. It may also cause an increase in the nucleation sites of gold nanoparticles. With regard to the smallest nanoparticle size with air-UFBs, sonochemically produced NO and/or NO_2^- might play some role [24,53]. Further studies are required on these topics.
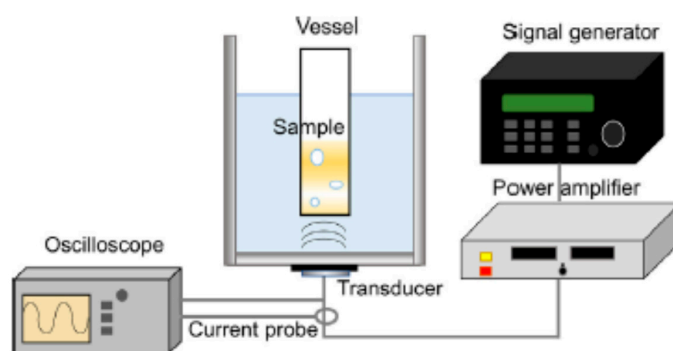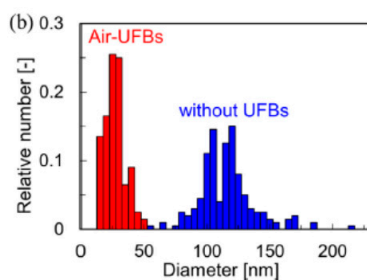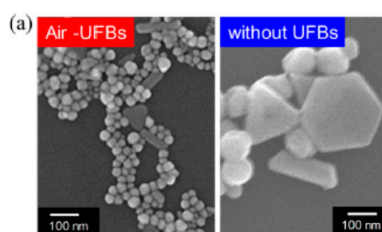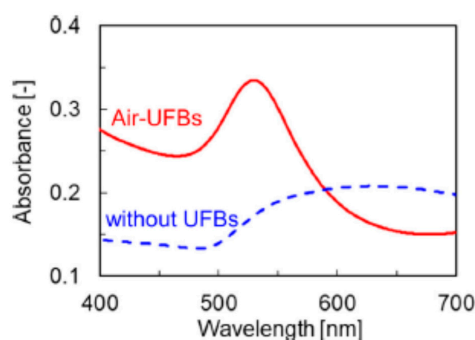
Figure 6. Sonochemical reduction of aqueous 0.1 mM $AuCl_4^-$ solutions by 495 kHz sonication for 10 min at 10 °C to produce gold nanoparticles with and without ultrafine bubbles. (**i**) Experimental apparatus. (**ii**) (**a**) SEM images of gold nanoparticles. (**b**) The size distribution of spherical gold nanoparticles. (**iii**) Absorption spectra. Reprinted with permission from Ref. [84]. Copyright 2020, Elsevier.

In 2002, Caruso et al. [68] recognized that sonochemical reduction of $AuCl_4^-$ occurred in 0.2 mM aqueous $AuCl_4^-$ solutions without any additives at 20 °C purged with argon for 15 min before sonication. In the experiment of Caruso et al. [68], an ultrasonic horn was used for sonication at 20 kHz for 2.5 min. Gold nanoparticles were produced without any additives such as alcohol, although not as much as when alcohol was added to the solution [68]. It can be seen from Figure 7 that the amount of reduced $AuCl_4^-$ was non-zero even in the absence of alcohols (at an alcohol concentration of zero) [68].
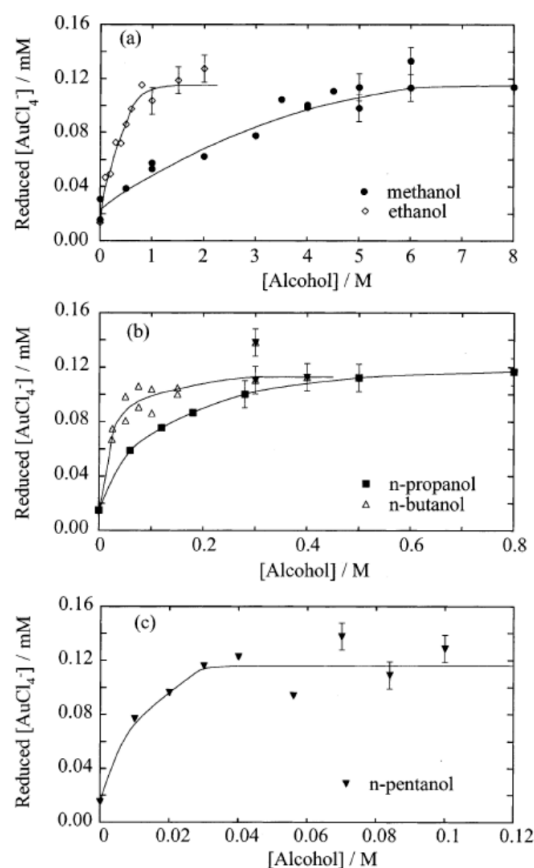
**Figure 7.** The amount of $AuCl_4^-$ reduced by sonication for 2.5 min as a function of the alcohol concentration for (**a**) methanol and ethanol, (**b**) 1-propanol and 1-butanol, and (**c**) 1-pentanol. The initial concentration of $AuCl_4^-$ was 0.2 mM. The pH of the solutions before and after sonication was between 3.1 and 3.5. The liquid temperature was maintained at 21 ± 3 °C. Reprinted with permission from Ref. [68]. Copyright 2002, the American Chemical Society.

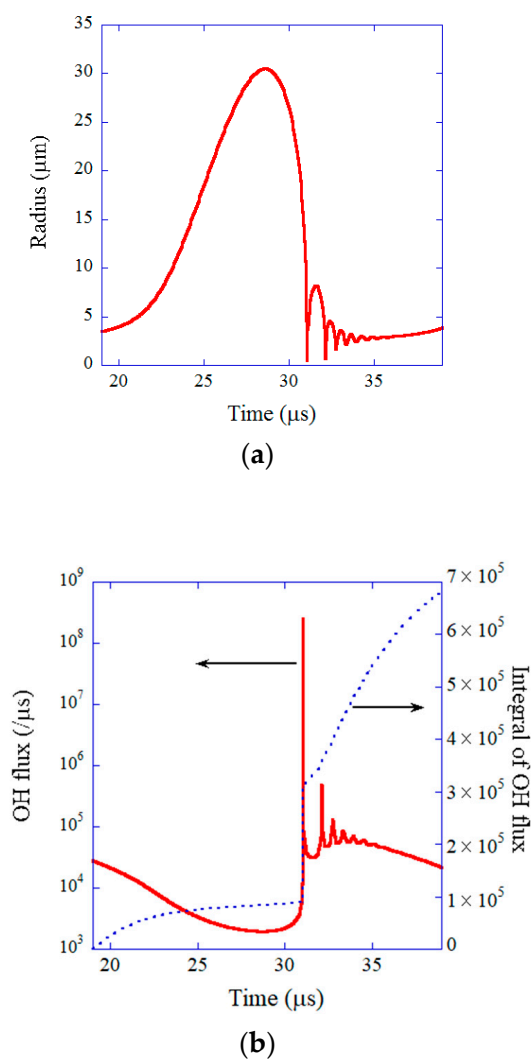### 3. Results of Numerical Simulations and Discussion

There are various theoretical models of bubble dynamics for numerical simulations of chemical reactions inside a cavitation bubble [2,16,19,24,53,77,80,100–117]. The first paper on numerical simulations of sonochemical reactions was probably by Kamath, Prosperetti, and Egolfopoulos in 1993 [100]. The model used in the numerical simulations discussed in the present paper is schematically shown in Figure 8 [116]. Temperature and pressure are assumed to be spatially uniform inside a bubble except at the thermal boundary layer near the bubble wall [2,16,19,24,53,77,80,111–117]. Non-equilibrium evaporation and condensation of water vapor take place at the bubble wall [115]. Thermal conduction takes place both inside and outside a bubble [19]. The temporal variation of liquid temperature at the bubble wall is numerically calculated using a rather simple model [112]. Non-equilibrium chemical reactions are taken into account by numerically calculating chemical reaction rates using Arrhenius-type rate constants [19,114]. For an air bubble, rates of 93 chemical reactions and their backward reactions are numerically calculated as a function of time involving N_2, O_2, H_2O, OH, H, O, HO_2, H_2O_2, O_3, N, HNO_2, HNO, HNO_3, NO, NO_2, and N_2O [114,118–120]. Kalmar et al. [105] pointed out that the results of numerical simulations strongly depend on the chemical kinetics model employed in the simulations. In the present model, the ionization of gases and vapor inside a heated bubble is taken into account, considering the ionization-potential lowering due to high density inside a bubble at the end of the violent bubble collapse [16,113]. The model has been validated through the study of single-bubble sonochemistry [24]. The single-bubble system is as follows. A single stably pulsating bubble is trapped near the pressure antinode of a stand-

ing ultrasonic wave due to the acoustic radiation force called the primary Bjerknes force in degassed water [17,32,121,122]. If the liquid water is not sufficiently degassed, many cavitation bubbles appear under the irradiation of strong ultrasound, and a single-bubble system cannot be obtained. Single-bubble sonoluminescence (SBSL) is the light emission phenomenon from the single-bubble system [2,17,27,32,111,122] and was a popular topic in scientific research soon after the report by Barber and Putterman in 1991 [123] on the extremely short pulse-width of SBSL. In 2002, Didenko and Suslick [124] experimentally reported the production rate of OH radicals from a SBSL bubble, which is called single-bubble sonochemistry.
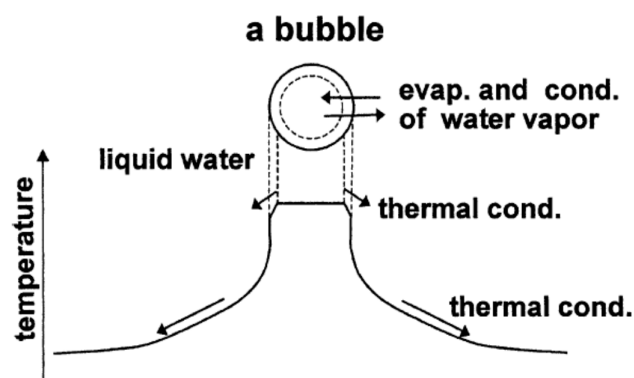

Figure 8. The model of bubble dynamics. The abscissa axis is spatial position. Reprinted with permission from Ref. [116]. Copyright 2004, Elsevier.
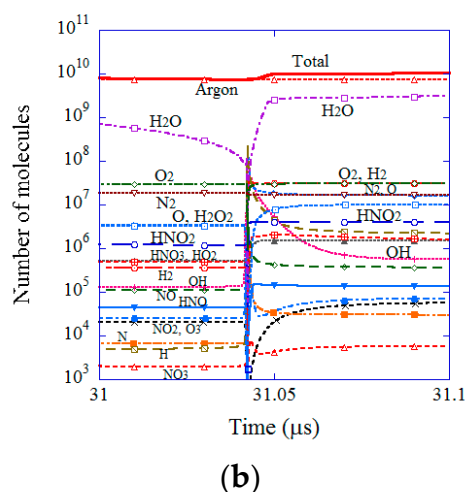
The results of numerical simulations under the condition of single-bubble sonochemistry are shown in Figures 9 and 10 [24]. During the rarefaction phase of ultrasound, a bubble expands to a maximum radius of 30.5 μm (Figure 9a) [24,124]. At the compression phase of ultrasound, a bubble violently collapses, which is the Rayleigh collapse. At the end of the violent collapse, the temperature and pressure inside a bubble increase to 10,900 K and 7.9×10^9 Pa, respectively (Figure 10a for temperature) [24]. As a result, almost all water vapor molecules inside a bubble are dissociated at the end of the violent bubble collapse, and an appreciable amount of OH radicals are produced inside the bubble (Figure 10b). It should be noted that the main content of a SBSL bubble is argon because nitrogen and oxygen chemically react inside a heated air bubble and change to HNO_x and NO_x, which gradually dissolve into the surrounding liquid water [17,125]. After about one hundred acoustic cycles, which corresponds to one hundred violent collapses, only chemically inactive argon remains inside a bubble, as 1% of the air in the molar fraction is argon [126]. This argon rectification hypothesis has been validated both theoretically and experimentally [17]. The chemical species present inside a SBSL bubble just before the end of the violent collapse in Figure 10b were produced at the previous violent collapse [24]. The OH flux from the SBSL bubble and its time integral are shown in Figure 9b as a function of time for one acoustic cycle [24]. About 1/3 of the total amount of OH radicals that diffuse into the surrounding liquid water in one acoustic cycle diffuse out of a bubble at around the end of the violent collapse. The other 2/3 of OH radicals diffuse into the surrounding liquid during bubble expansion and the bouncing motion shown in Figure 9a. The total amount of OH radicals that diffuse into the liquid is 6.6×10^5 in number of molecules according to the present numerical simulation, which almost agrees with the experimental data of 8.2×10^5 by Didenko and Suslick [124]. It means that the present model has been validated by comparison with the experimental data. It should be noted that an ODE (ordinary differential equations) model like the present model needs to be validated through comparison with experimental data or the results of first-principle calculations because an ODE model is not fully based on the first principles [127].

(a)

(b)

Figure 9. The results of the numerical simulations under the experimental condition of single-bubble sonochemistry as a function of time for one acoustic cycle under ultrasound of 52 kHz and 1.52 bar in water at 3 °C. (**a**) The bubble radius. (**b**) The dissolution rate of OH radicals into the liquid water from the interior of the bubble (red solid line) and its time integral (blue dotted line). Reprinted with permission from Ref. [24]. Copyright 2005, AIP Publishing.

(a)

Figure 10. *Cont.*

(b)
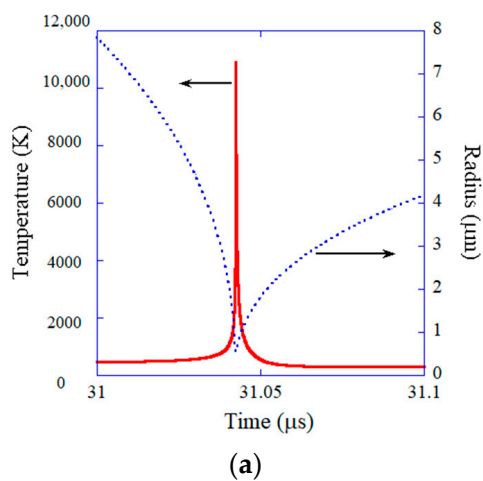
Figure 10. The results of the numerical simulations for a SBSL bubble (mostly an argon bubble) as a function of time at around the end of the violent bubble collapse under ultrasound of 52 kHz and 1.52 bar. (**a**) The bubble radius and the temperature inside the bubble. (**b**) The number of molecules inside the bubble. Reprinted with permission from Ref. [24]. Copyright 2005, AIP Publishing.

The amounts of chemical products that dissolve into the surrounding liquid from a SBSL bubble (mostly an argon bubble) in one acoustic cycle are shown in Table 1, according to the results of the numerical simulation [24]. In order to discuss reducing agents produced from a SBSL bubble, the reduction potentials of reducing agents are listed in Table 2 [128–130]. Among the reducing agents produced from a SBSL bubble in Table 1, the reduction potential of the H atom is extremely high, as listed in Table 2. In other words, the main reducing agent produced by a SBSL bubble is the H atom. For an air bubble, the amount of H atoms produced from a bubble is much smaller than that from an argon bubble (a SBSL bubble), as listed in Table 3. Nevertheless, as the reduction potential of H atoms is extremely high compared to other reducing agents, the main reducing agent produced from an air bubble would also be H atoms. Experimentally, H atoms produced from argon-saturated aqueous solutions irradiated with ultrasound (which are multi-bubble systems) have been detected by spin trapping and electron spin resonance along with OH radicals [131–133].

Table 1. The amounts of chemical products that dissolve into the liquid water from the interior of a SBSL bubble (mostly an argon bubble) in one acoustic cycle according to the numerical simulation. The liquid volume in the experiment [124] was about 15 mL. Reprinted with permission from Ref. [24]. Copyright 2005, AIP Publishing.

Chemical Species	Number of Molecules per Acoustic Cycle
H_2	3.1×10^7
O	1.3×10^7
H_2O_2	6.3×10^6
H	4.1×10^6
HNO_2	2.3×10^6
HO_2	1.1×10^6
HNO_3	8.4×10^5
OH	6.6×10^5
NO	2.5×10^5
HNO	9.5×10^4
NO_2	4.4×10^4
O_3	3.4×10^4
N	2.9×10^4
NO_3	3.1×10^3
N_2O	3.1×10^2

Table 2. The reduction potentials of reducing agents [128–130].

Reducing Agent	Reaction	Reduction Potential (V)
e^-(aq)	e^-(aq) $\rightarrow e^-$	2.88 [128]
H(aq)	H(aq) $\rightarrow H^+ + e^-$	2.31 [128]
H_2	$H_2 + 2OH^- \rightarrow 2H_2O + 2e^-$	0.83 [129] [1]
CH_2OH	$CH_2OH \rightarrow CHOH + H^+ + e^-$	0.73 [130]
CH_3CHOH	$CH_3CHOH \rightarrow CH_3COH + H^+ + e^-$	0.69 [130]
O_2^-	$O_2^- \rightarrow O_2$(aq) $+ e^-$	0.18 [128]
CO	$CO + H_2O \rightarrow CO_2 + 2H^+ + 2e^-$	0.11 [129]
HO_2	$HO_2 \rightarrow O_2 + H^+ + e^-$	0.05 [129]
H_2	$H_2 \rightarrow 2H^+ + 2e^-$	0.00 [129]
NO_2^-	$NO_2^- + 2OH^- \rightarrow NO_3^- + H_2O + 2e^-$	-0.01 [129] [1]
NO	$NO + 2OH^- \rightarrow NO_2^- + H_2O + e^-$	-0.46 [129] [1]
HNO_2	$2HNO_2 \rightarrow NO + NO_3^- + 2H^+ + e^-$	-0.52 [129]
I^-	$3I^- \rightarrow I_3^- + 2e^-$	-0.54 [129]
H_2O_2	$H_2O_2 \rightarrow O_2 + 2H^+ + 2e^-$	-0.70 [129]
NO	$NO + H_2O \rightarrow NO_2 + 2H^+ + 2e^-$	-1.05 [129]

[1] $\left[OH^-\right] \approx 1 \text{ mol L}^{-1}$.

Table 3. The amounts of chemical products that dissolve into the liquid water from the interior of an initial air bubble in one acoustic cycle according to the numerical simulation. Reprinted with permission from Ref. [24]. Copyright 2005, AIP Publishing.

Chemical Species	Number of Molecules per Acoustic Cycle
HNO_2	4.0×10^7
HNO_3	3.7×10^7
O	1.6×10^7
H_2O_2	5.1×10^6
O_3	2.7×10^6
HO_2	2.3×10^6
NO_3	1.1×10^6
H_2	1.0×10^6
OH	9.9×10^5
NO_2	3.9×10^5
N_2O	3.0×10^5
NO	1.3×10^5
H	1.1×10^5
HNO	2.8×10^4
N	2.7×10^3
N_2O_5	6.8×10^2

For a SBSL bubble (mostly an argon bubble), the main chemical product produced from a bubble is H_2 as shown in Table 1 [24]. Indeed, H_2 produced from cavitation bubbles in water under argon irradiated with 300 kHz and 12 W of ultrasound (which was a multi-bubble system) was experimentally detected by using a mass spectrometer, and the rate of H_2 formation was 10 μM min^{-1} [134]. There are also other experimental reports that H_2 produced from cavitation bubbles in water in which O_2, air, N_2, or argon were dissolved and irradiated with ultrasound was detected [23,70,135–137]. There have also been some numerical studies on the hydrogen production from cavitation bubbles in recent years [138–141]. In the experiment of Sakai et al. [70], H_2-gas purging alone did not reduce $AuCl_4^-$ in aqueous solutions. Thus, the reducing power of H_2 is insufficient for the reduction of $AuCl_4^-$ as the reduction potential of H_2 in acidic solutions, which was the case in the experiments of Sakai et al. [69,70], is only 0.00 V (the standard condition) (Table 2). On the other hand, in strongly alkaline solutions, the reduction potential of H_2 could be larger than that of CH_2OH and CH_3CHOH, which easily reduce $AuCl_4^-$ (Table 2). It suggests that H_2 produced from cavitation bubbles could work as a reducing agent in strongly alkaline solutions. H_2 is also produced from an air bubble, as listed in Table 3.

For an air bubble, the main chemical product is HNO_2 under the conditions listed in Table 3 [24]. Indeed, HNO_2 produced from air bubbles in water at 25 °C irradiated with 447 kHz and 50 W ultrasound (which was a multi-bubble system) was detected by a diazotization method, and the rate of HNO_2 formation was 22 μM min^{-1} [142]. There have also been other experimental reports that NO_2^-, which is mainly formed by $HNO_2 \rightarrow H^+ + NO_2^-$ (pK = 3.3 [143]), produced from cavitation bubbles in water irradiated with ultrasound, is detected [23,124,136,144,145]. Although the reduction potential of HNO_2 in acidic solutions is rather low, as listed in Table 2, that of NO_2^- in strongly alkaline solutions is comparable to that of H_2 in acidic solutions. Further studies are required to determine whether HNO_2 and NO_2^- play some role in the sonochemical reduction of solutes. It should be noted that HNO_2 and NO_2^- not only work as reducing agents but also as oxidants, as listed in Table 4 [129,146].

**Table 4.** The oxidation potentials of oxidants [129,146].

Oxidant	Reaction	Oxidation Potential (V)
OH	$OH + H^+ + e^- \rightarrow H_2O$	2.81 [126]
O	$O + 2H^+ + 2e^- \rightarrow H_2O$	2.42 [126]
O_3	$O_3 + 2H^+ + 2e^- \rightarrow O_2 + H_2O$	2.07 [126]
H_2O_2	$H_2O_2 + 2H^+ + 2e^- \rightarrow 2H_2O$	1.78 [126]
NO_2^-	$2NO_2^- + 6H^+ + 4e^- \rightarrow N_2O + 3H_2O$	1.40 [116]
HNO_2	$2HNO_2 + 4H^+ + 4e^- \rightarrow N_2O + H_2O$	1.30 [116]
NO_2^-	$NO_2^- + 2H^+ + e^- \rightarrow NO + H_2O$	1.20 [116]
HNO_2	$HNO_2 + H^+ + e^- \rightarrow NO + H_2O$	1.00 [116]
$AuCl_4^-$	$AuCl_4^- + 3e^- \rightarrow Au + 4Cl^-$	1.00 [116]

Both for an argon bubble (a SBSL bubble) and an air bubble, one of the main chemical products is H_2O_2, as listed in Tables 1 and 3 [24]. Indeed, H_2O_2 produced from air bubbles in water at 25 °C irradiated with 447 kHz and 50 W ultrasound was detected by the oxidation reaction of potassium iodide (KI), and the rate of H_2O_2 formation was 21 μM min^{-1} [142]. A similar rate of H_2O_2 formation from argon bubbles was also experimentally reported [23]. Although H_2O_2 plays an important role in the sonochemical oxidation of solutes [23,51,52], Okitsu et al. [147] experimentally reported that H_2O_2 sometimes works as a reducing agent, such as in the following reaction.

$$2MnO_4^- + 3H_2O_2 \rightarrow 2MnO_2 + 3O_2 + 2OH^- + 2H_2O \tag{15}$$
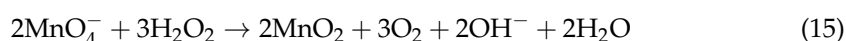
The chemical reaction (15) was confirmed to occur by the addition of H_2O_2 to a 0.1 mM $KMnO_4$ aqueous solution without ultrasonic irradiation [147]. As the reduction potential of H_2O_2 is the lowest among the reducing agents listed in Table 2 except NO in acidic solutions, almost all the reducing agents produced from cavitation bubbles, such as H_2, HO_2 (which becomes superoxide anion (O_2^-) in liquid water), HNO_2 (which becomes NO_2^- in liquid water), and NO (in strongly alkaline solutions), could possibly play some role in the sonochemical reduction of some solutes. It should be noted, however, that NO in acidic solutions does not reduce $AuCl_4^-$ because the reduction potential is even lower than (−1) times the oxidation potential of $AuCl_4^-$, as listed in Tables 2 and 4 [128–130,146].

The hydroperoxyl radical (HO_2) becomes a superoxide anion (O_2^-) in liquid water as follows [148].

$$HO_2 \leftrightarrow O_2^- + H^+ \quad pK = 4.8 \tag{16}$$
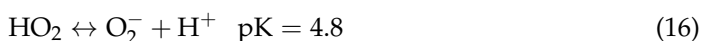
Kondo et al. [149] experimentally reported that HO_2 was detected in oxygen-saturated aqueous solutions irradiated by 50 kHz ultrasound and that there was evidence of O_2^- formation. There have been a few other experimental reports on the formation of superoxide anion (O_2^-) in liquid water irradiated by ultrasound [150,151]. However, the role of the superoxide anion (O_2^-) in the sonochemical reduction of solutes is still unclear, and further studies are required on this topic. As the reduction potential of O_2^- is higher than that

of CO, which has been reported to reduce metal ions [76] (Table 2), it is possible that the superoxide anion (O_2^-) plays some role in the sonochemical reduction of some solutes.

Finally, the role of hydrated electrons (e^-(aq)) produced from cavitation bubbles is discussed. In strongly alkaline solutions, hydrated electrons (e^-(aq)) are formed from H atoms as follows [23,81,152].

$$H + OH^- \leftrightarrow H_2O + e^-(aq) \quad pK = 9.8 \tag{17}$$
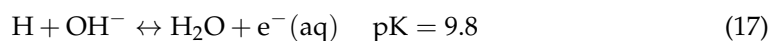
As the reduction potential of hydrated electrons is very high (Table 2), the reduction of thallium ions was experimentally reported in strongly alkaline solutions in which an argon-hydrogen mixture was dissolved and irradiated with 1 MHz ultrasound as follows [23,81].

$$Tl^+ + e^-(aq) \rightarrow Tl^0 \tag{18}$$

As a result, colloidal thallium was formed. Thallium ions were not reduced in neutral or weakly alkaline solutions [23,81]. On the other hand, hydrated electrons (e^-(aq)) are possibly produced from plasma formed inside heated cavitation bubbles as there are free electrons in the plasma [2,12,16,17,20,24,26–32,103,109,113,153–155]. At present, however, hydrated electrons (e^-(aq)) have been experimentally detected only from a moving SBSL bubble in neutral or acidic solutions [29,156]. In a multi-bubble system at neutral pH, no detectable yield of hydrated electrons in argon-saturated aqueous solutions irradiated with 50 kHz ultrasound at 20 °C was found experimentally [157]. Further studies are required on the role of hydrated electrons in the sonochemical reduction of solutes.

Next, the dependence of amounts of chemical species produced from a cavitation bubble on ultrasonic frequency is discussed based on numerical simulations of chemical reactions inside an air bubble [53]. For relatively low ultrasonic frequencies (20 and 100 kHz), there is a peak in bubble temperature at the violent bubble collapse as a function of the pressure amplitude of ultrasound (acoustic amplitude), as shown in Figure 11a [53]. The reason is that for relatively low ultrasonic frequencies, the bubble content becomes mostly water vapor at the end of the violent bubble collapse at a relatively high acoustic amplitude because a bubble dramatically expands during the rarefaction phase of ultrasound and intense evaporation of water vapor occurs during the bubble expansion. When the bubble content is mostly water vapor, which is called a vaporous bubble, the bubble temperature at the violent collapse does not increase much because the endothermic dissociation of water vapor cools the bubble considerably [19,113,158,159]. Although the bubble collapse becomes more violent as the acoustic amplitude increases, the bubble temperature decreases for relatively high acoustic amplitudes due to the increase in the amount of water vapor trapped inside a collapsing bubble, as shown in Figure 11b [53]. This is the reason for the appearance of the peak in bubble temperature as a function of acoustic amplitude at relatively low ultrasonic frequencies. For relatively high ultrasonic frequencies (300 kHz and 1 MHz), on the other hand, the amount of water vapor trapped inside a bubble at the end of the bubble collapse is much smaller than that at relatively low ultrasonic frequencies, and thus the bubble temperature increases as the acoustic amplitude increases until it reaches a plateau as shown in Figure 11a,b [53].

When the bubble temperature is higher than about 7000 K, oxidants such as OH, O, H_2O_2, and O_3 are strongly consumed inside an air bubble by oxidizing nitrogen [2,53,111,116]. In addition, H atoms are also strongly consumed inside an air bubble at such a high temperature by the following chemical reactions; $H + O_2 \rightarrow O + OH$, $H + O_2 + M \rightarrow HO_2 + M$, $H + OH \rightarrow H_2 + O$, $H + HNO_2 \rightarrow H_2 + NO_2$, and $H + NO_2 \rightarrow NO + OH$ [53]. As a result, the main chemical products at such a high temperature are HNO_2, NO, HNO_3, H_2, and NO_2, as seen in Figure 12 [53].
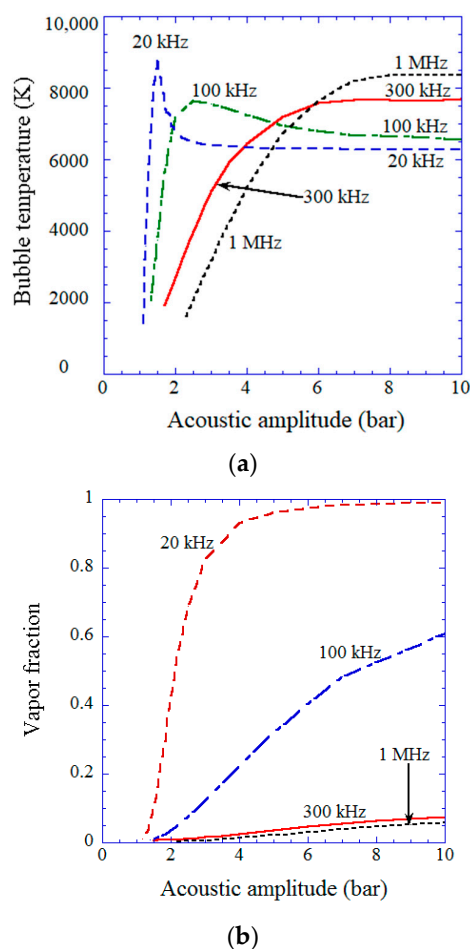
Figure 11. The results of the numerical simulations as a function of acoustic pressure amplitude for various ultrasonic frequencies for the first collapse of an isolated air bubble. (**a**) The temperature inside a bubble at the violent collapse. (**b**) The molar fraction of water vapor inside a bubble at the end of the violent collapse. Reprinted with permission from Ref. [53]. Copyright 2007, AIP Publishing.

In an ultrasonic bath, a standing wave of ultrasound is formed because ultrasound is strongly reflected by the liquid surface [2,160]. In a standing wave field, bubbles are repelled from high-acoustic-amplitude regions due to the acoustic radiation force called the primary Bjerknes force [2,121]. For example, at 20 kHz, bubbles are repelled from regions with a higher acoustic amplitude than about 1.75 bar [121,161]. In regions with a smaller acoustic amplitude than about 1.75 bar, bubbles are attracted toward the higher-acoustic-amplitude regions. Accordingly, many bubbles gather around the region with an acoustic amplitude of about 1.75 bar. Indeed, the structure of bubbles has been experimentally observed, which is sometimes called the jellyfish structure [162,163]. At about 1.75 bar at 20 kHz, the bubble temperature is higher than about 7000 K, according to Figure 11 [53]. It means that the amount of H atoms produced in an ultrasonic bath at 20 kHz is extremely small, as seen in Figure 12a [53]. It may be the reason why the rate of sonochemical reduction of $AuCl_4^-$ at 28 kHz is much lower than those at 200 and 950 kHz (Figure 1), according to Sakai et al. [69]. On the other hand, if an ultrasonic horn is used at 20 kHz, it is predicted that the amount of H atoms produced from an air bubble is much larger because the acoustic amplitude is much higher, according to Figure 12a [53,159]. However, it should be noted that under an ultrasonic horn, the bubble-bubble interaction, which is the influence of acoustic emissions of surrounding bubbles on bubble pulsation, is very strong and that the effect of the bubble-bubble interaction should be taken into account in the numerical simulations of chemical reactions inside cavitation bubbles [164,165]. Further studies are required on this topic.
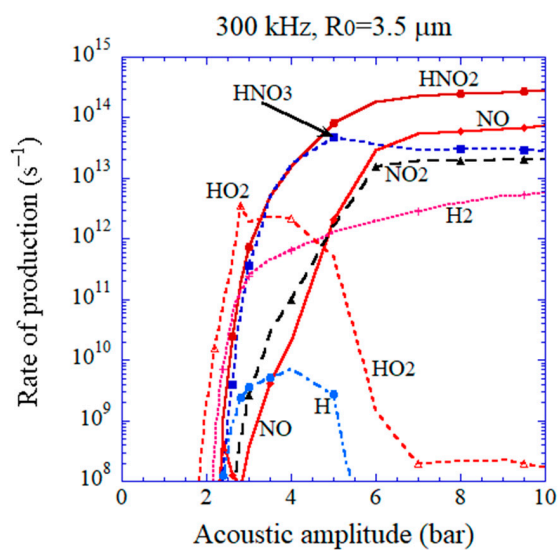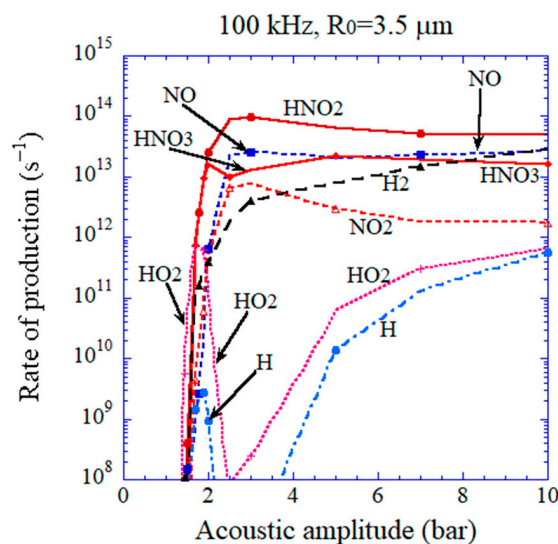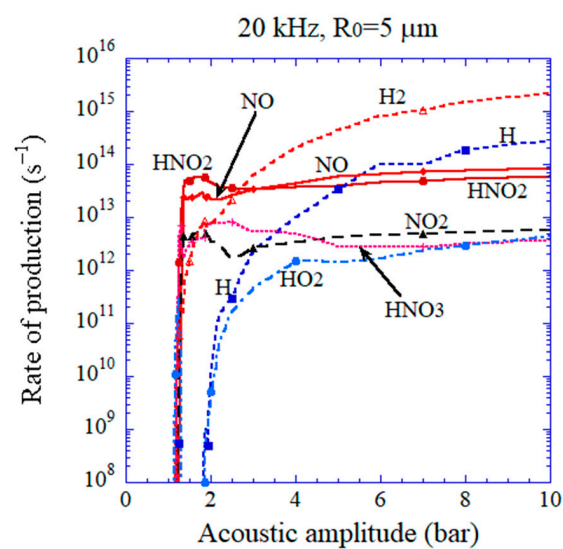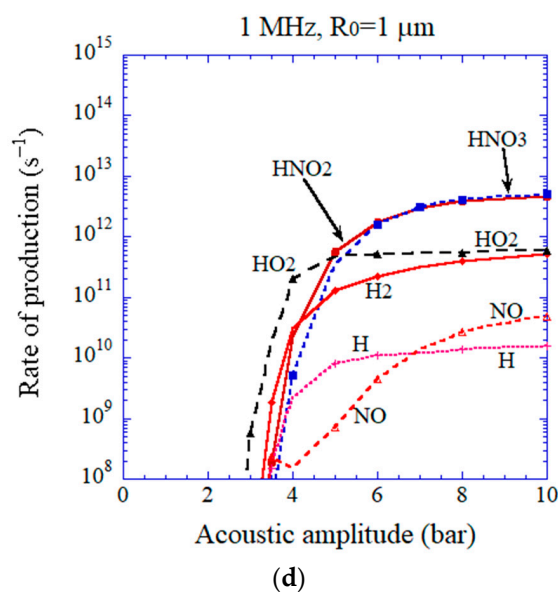
(**a**)

(**b**)

(**c**)

Figure 12. *Cont.*

Figure 12. The results of the numerical simulations on the rate of production of chemical species other than oxidants inside an isolated air bubble as a function of acoustic pressure amplitude. (**a**) 20 kHz, (**b**) 100 kHz, (**c**) 300 kHz, (**d**) 1 MHz. Reprinted with permission from Ref. [53]. Copyright 2007, AIP Publishing.

Finally, the challenges faced in this field are summarized, and the outlook for the research direction is discussed. The roles of H_2, NO_2^-, HNO_2, H_2O_2, O_2^-, HO_2, and hydrated electrons ($e^-(aq)$) in the sonochemical reduction of solutes without any additives need to be studied in more detail. The mechanism of sonochemical reduction of carbon dioxide experimentally reported recently [166] needs to be studied in more detail. Based on the detailed mechanism, conditions to enhance the sonochemical reduction of solutes need to be clarified, such as ultrasonic frequency, acoustic amplitude, type of sonochemical reactor (bath or horn), pH, etc. It will hopefully lead to industrial applications of sonochemical reduction as well as oxidation because it is a green process [167–169]. The same is true for chemical reactions induced by hydrodynamic cavitation (sometimes called fine-bubble technology) [170–174].

4. Conclusions

It is experimentally reported that reduction of $AuCl_4^-$ occurs in aqueous solutions without any additives such as organic materials irradiated with strong ultrasound, although oxidation reactions occur in most sonochemical reactions. Considering the high reduction potential of H atoms, the main reducing agent produced from cavitation bubbles under ultrasound in water without any additives is a H atom, according to the numerical simulations of chemical reactions inside an air or argon bubble under ultrasound. In strongly alkaline solutions, H_2 produced from cavitation bubbles could also work as a reducing agent. Hydrated electrons ($e^-(aq)$), which could be formed from H atoms in strongly alkaline solutions, may also work as a reducing agent. Superoxide anion (O_2^-), which is formed from HO_2 produced from cavitation bubbles in aqueous solutions, could possibly work as a reducing agent. Further studies are required on the role of HNO_2 in the sonochemical reduction of some solutes. The outlook for research direction is also discussed.

References

1. Fuchs, F.J. Ultrasonic cleaning and washing of surfaces. In *Power Ultrasonics*; Gallego-Juarez, J.A., Graff, K.F., Eds.; Elsevier: Amsterdam, The Netherlands, 2015; pp. 577–609.
2. Yasui, K. *Acoustic Cavitation and Bubble Dynamics*; Springer: Cham, Switzerland, 2018.
3. Asadi, A.; Pourfattah, F.; Szilágyi, I.M.; Afrand, M.; Żyła, G.; Ahn, H.S.; Wongwises, S.; Nguyen, H.M.; Arabkoohsar, A.; Mahian, O. Effect of sonication characteristics on stability, thermophysical properties, and heat transfer of nanofluids: A comprehensive review. *Ultrason. Sonochem.* **2019**, *58*, 104701. [CrossRef] [PubMed]
4. Graves, J.E.; Sugden, M.; Litchfield, R.E.; Hutt, D.A.; Mason, T.J.; Cobley, A.J. Ultrasound assisted dispersal of a copper nanopowder for electroless copper activation. *Ultrason. Sonochem.* **2016**, *29*, 428–438. [CrossRef] [PubMed]
5. Lv, Y.-Z.; Li, C.; Sun, Q.; Huang, M.; Li, C.-R.; Qi, B. Effect of dispersion method on stability and dielectric strength of transformer oil-based TiO$_2$ nanofluids. *Nanoscale Res. Lett.* **2016**, *11*, 515. [CrossRef]
6. Hwang, Y.; Lee, J.-K.; Lee, J.-K.; Jeong, Y.-M.; Cheong, S.-I.; Ahn, Y.-C.; Kim, S.H. Production and dispersion stability of nanoparticles in nanofluids. *Powder Technol.* **2008**, *186*, 145–153. [CrossRef]
7. Sato, K.; Li, J.-G.; Kamiya, H.; Ishigaki, T. Ultrasonic dispersion of TiO$_2$ nanoparticles in aqueous suspension. *J. Am. Ceram. Soc.* **2008**, *91*, 2481–2487. [CrossRef]
8. Sauter, C.; Emin, M.A.; Schuchmann, H.P.; Tavman, S. Influence of hydrostatic pressure and sound amplitude on the ultrasound induced dispersion and de-agglomeration of nanoparticles. *Ultrason. Sonochem.* **2008**, *15*, 517–523. [CrossRef]
9. Yasui, K.; Towata, A.; Tuziuti, T.; Kozuka, T.; Kato, K. Effect of static pressure on acoustic energy radiated by cavitation bubbles in viscous liquids under ultrasound. *J. Acoust. Soc. Am.* **2011**, *130*, 3233–3242. [CrossRef]
10. Yasui, K.; Kato, K. Numerical simulations of sonochemical production and oriented aggregation of BaTiO$_3$ nanocrystals. *Ultrason. Sonochem.* **2017**, *35*, 673–680. [CrossRef]
11. Iida, Y.; Tuziuti, T.; Yasui, K.; Towata, A.; Kozuka, T. Control of viscosity in starch and polysaccharide solutions with ultrasound after gelatinization. *Innov. Food Sci. Emerg. Technol.* **2008**, *9*, 140–146. [CrossRef]
12. Yasui, K. Multibubble sonoluminescence from a theoretical perspective. *Molecules* **2021**, *26*, 4624. [CrossRef]
13. Weninger, K.R.; Camara, C.G.; Putterman, S.J. Observation of bubble dynamics within luminescent cavitation clouds: Sonoluminescence at the nano-scale. *Phys. Rev. E* **2001**, *63*, 016310. [CrossRef] [PubMed]
14. Lee, J.; Ashokkumar, M.; Kentish, S.; Grieser, F. Determination of the size distribution of sonoluminescence bubbles in a pulsed acoustic field. *J. Am. Chem. Soc.* **2005**, *127*, 16810–16811. [CrossRef] [PubMed]
15. Brotchie, A.; Grieser, F.; Ashokkumar, M. Effect of power and frequency on bubble-size distributions in acoustic cavitation. *Phys. Rev. Lett.* **2009**, *102*, 084302. [CrossRef] [PubMed]
16. Yasui, K.; Tuziuti, T.; Lee, J.; Kozuka, T.; Towata, A.; Iida, Y. The range of ambient radius for an active bubble in sonoluminescence and sonochemical reactions. *J. Chem. Phys.* **2008**, *128*, 184705. [CrossRef] [PubMed]
17. Brenner, M.P.; Hilgenfeldt, S.; Lohse, D. Single-bubble sonoluminescence. *Rev. Mod. Phys.* **2002**, *74*, 425–484. [CrossRef]
18. Yasui, K. Dynamics of acoustic bubbles. In *Sonochemistry and the Acoustic Bubble*; Grieser, F., Choi, P.-K., Enomoto, N., Harada, H., Okitsu, K., Yasui, K., Eds.; Elsevier: Amsterdam, The Netherlands, 2015; pp. 41–83.
19. Yasui, K. Alternative model of single-bubble sonoluminescence. *Phys. Rev. E* **1997**, *56*, 6750–6760. [CrossRef]
20. Suslick, K.S.; Eddingsaas, N.C.; Flannigan, D.J.; Hopkins, S.D.; Xu, H. The chemical history of a bubble. *Acc. Chem. Res.* **2018**, *51*, 2169–2178. [CrossRef]
21. Didenko, Y.T.; McNamara, W.B., III; Suslick, K.S. Temperature of multibubble sonoluminescence in water. *J. Phys. Chem. A* **1999**, *103*, 10783–10788. [CrossRef]
22. McNamara, W.B., III; Didenko, Y.T.; Suslick, K.S. Pressure during sonoluminescence. *J. Phys. Chem. B* **2003**, *107*, 7303–7306. [CrossRef]
23. Henglein, A. Contributions to various aspects of cavitation chemistry. In *Advances in Sonochemistry*; Mason, T.J., Ed.; JAI Press: London, UK, 1993; Volume 3, pp. 17–83.
24. Yasui, K.; Tuziuti, T.; Sivakumar, M.; Iida, Y. Theoretical study of single-bubble sonochemistry. *J. Chem. Phys.* **2005**, *122*, 224706. [CrossRef]
25. Yasui, K. Production of O radicals from cavitation bubbles under ultrasound. *Molecules* **2022**, *27*, 4788. [CrossRef] [PubMed]
26. Choi, P. Sonoluminescence. In *Sonochemistry and the Acoustic Bubble*; Grieser, F., Choi, P.-K., Enomoto, N., Harada, H., Okitsu, K., Yasui, K., Eds.; Elsevier: Amsterdam, The Netherlands, 2015; pp. 85–117.
27. Young, F.R. *Sonoluminescence*; CRC Press: Boca Raton, FL, USA, 2005.
28. Nikitenko, S.I.; Pflieger, R. Toward a new paradigm for sonochemistry: Short review on nonequilibrium plasma observations by means of MBSL spectroscopy in aqueous solutions. *Ultrason. Sonochem.* **2017**, *35*, 623–630. [CrossRef]
29. Sharipov, G.L.; Gareev, B.M.; Abdrakhmanov, A.M. Confirmation of hydrated electrons formation during the moving single-bubble sonolysis: Activation of Tb^{3+} ion sonoluminescence by e$_{aq}^-$ acceptors in an aqueous solution. *J. Photochem. Photobiol. A* **2020**, *402*, 112800. [CrossRef]

30. Suslick, K.S.; Eddingsaas, N.C.; Flannigan, D.J.; Hopkins, S.D.; Xu, H. Extreme conditions during multibubble cavitation: Sonoluminescence as a spectroscopic probe. *Ultrason. Sonochem.* **2011**, *18*, 842–846. [CrossRef]

31. Choi, P.-K. Sonoluminescence and acoustic cavitation. *Jpn. J. Appl. Phys.* **2017**, *56*, 07JA01. [CrossRef]

32. Yasui, K.; Tuziuti, T.; Sivakumar, M.; Iida, Y. Sonoluminescence. *Appl. Spectrosc. Rev.* **2004**, *39*, 399–436. [CrossRef]

33. Grieser, F.; Choi, P.-K.; Enomoto, N.; Harada, H.; Okitsu, K.; Yasui, K. (Eds.) *Sonochemistry and the Acoustic Bubble*; Elsevier: Amsterdam, The Netherlands, The Netherlands, 2015.

34. Chen, D.; Sharma, S.K.; Mudhoo, A. (Eds.) *Handbook on Applications of Ultrasound Sonochemistry for Sustainability*; CRC Press: Boca Raton, FL, USA, 2012.

35. Ashokkumar, M.; Cavalieri, F.; Chemat, F.; Okitsu, K.; Sambandam, A.; Yasui, K.; Zisu, B. (Eds.) *Handbook of Ultrasonics and Sonochemistry*; Springer: Singapore, 2016; Volumes 1–2.

36. Petrier, C. The use of power ultrasound for water treatment. In *Power Ultrasonics*; Gallego-Juarez, J.A., Graff, K.F., Eds.; Elsevier: Amsterdam, The Netherlands, 2015; pp. 939–972.

37. Mason, T.J.; Lorimer, J.P. *Sonochemistry: Theory, Applications and Uses of Ultrasound in Chemistry*; Ellis Horwood: Chichester, UK, 1988.

38. Mason, T.J. *Sonochemistry*; Oxford University Press: Oxford, UK, 1999.

39. Serna-Galvis, E.A.; Porras, J.; Torres-Palma, R.A. A critical review on the sonochemical degradation of organic pollutants in urine, seawater, and mineral water. *Ultrason. Sonochem.* **2022**, *82*, 105861. [CrossRef]

40. McMurray, H.N.; Wilson, B.P. Mechanistic and spatial study of ultrasonically induced luminol chemiluminescence. *J. Phys. Chem. A* **1999**, *103*, 3955–3962. [CrossRef]

41. Hatanaka, S.; Yasui, K.; Tuziuti, T.; Mitome, H. Difference in threshold between sono- and sonochemical luminescence. *Jpn. J. Appl. Phys.* **2000**, *39*, 2962–2966. [CrossRef]

42. Ashokkumar, M.; Lee, J.; Iida, Y.; Yasui, K.; Kozuka, T.; Tuziuti, T.; Towata, A. Spatial distribution of acoustic cavitation bubbles at different ultrasound frequencies. *ChemPhysChem* **2010**, *11*, 1680–1684. [CrossRef]

43. Rivas, D.F.; Ashokkumar, M.; Leong, T.; Yasui, K.; Tuziuti, T.; Kentish, S.; Lohse, D.; Gardeniers, H.J.G.E. Sonoluminescence and sonochemiluminescence from a microreactor. *Ultrason. Sonochem.* **2012**, *19*, 1252–1259. [CrossRef]

44. Yasuda, K.; Torii, T.; Yasui, K.; Iida, Y.; Tuziuti, T.; Nakamura, M.; Asakura, Y. Enhancement of sonochemical reaction of terephthalate ion by superposition of ultrasonic fields of various frequencies. *Ultrason. Sonochem.* **2007**, *14*, 699–704. [CrossRef] [PubMed]

45. Sunartio, D.; Yasui, K.; Tuziuti, T.; Kozuka, T.; Iida, Y.; Ashokkumar, M.; Grieser, F. Correlation between Na* emission and "chemically active" acoustic cavitation bubbles. *ChemPhysChem* **2007**, *8*, 2331–2335. [CrossRef] [PubMed]

46. Tuziuti, T.; Yasui, K.; Lee, J.; Kozuka, T.; Towata, A.; Iida, Y. Mechanism of enhancement of sonochemical-reaction efficiency by pulsed ultrasound. *J. Phys. Chem. A* **2008**, *112*, 4875–4878. [CrossRef] [PubMed]

47. Tsukahara, K.; Umemura, S.-I.; Yoshizawa, S. Effect of ultrasonic intensity and intervals of ultrasonic exposure on efficiency of sonochemiluminescence in gel phantom for sonodynamic therapy. *Jpn. J. Appl. Phys.* **2021**, *60*, SDDE12. [CrossRef]

48. Choi, P.-K.; Akiu, T.; Minowa, S.; Kim, J.; Kim, M. Cavitation threshold pressure of focused ultrasound observed with sonochemiluminescence. *Jpn. J. Appl. Phys.* **2022**, *61*, SG1003. [CrossRef]

49. Du, F.; Ma, X.; Yuan, F.; Wang, C.; Snizhko, D.; Guan, Y.; Xu, G. Sonochemiluminescence based on a small, cheap, and low-power USB mesh-type piezoelectric ultrasonic transducer. *Anal. Chem.* **2020**, *92*, 4755–4759. [CrossRef]

50. Lee, J.; Hallez, L.; Touyeras, F.; Ashokkumar, M.; Hihn, J.-Y. Influence of frequency sweep on sonochemiluminescence and sonoluminescence. *Ultrason. Sonochem.* **2020**, *64*, 105047. [CrossRef]

51. Koda, S.; Kimura, T.; Kondo, T.; Mitome, H. A standard method to calibrate sonochemical efficiency of an individual reaction system. *Ultrason. Sonochem.* **2003**, *10*, 149–156. [CrossRef]

52. Iida, Y.; Yasui, K.; Tuziuti, T.; Sivakumar, M. Sonochemistry and its dosimetry. *Microchem. J.* **2005**, *80*, 159–164. [CrossRef]

53. Yasui, K.; Tuziuti, T.; Kozuka, T.; Towata, A.; Iida, Y. Relationship between the bubble temperature and main oxidant created inside an air bubble under ultrasound. *J. Chem. Phys.* **2007**, *127*, 154502. [CrossRef] [PubMed]

54. Okitsu, K.; Cavalieri, F. *Sonochemical Production of Nanomaterials*; Springer: Cham, Switzerland, 2018.

55. Enomoto, N.; Okitsu, K. Application of ultrasound in inorganic synthesis. In *Sonochemistry and the Acoustic Bubble*; Grieser, F., Choi, P.-K., Enomoto, N., Harada, H., Okitsu, K., Yasui, K., Eds.; Elsevier: Amsterdam, The Netherlands, 2015; pp. 187–206.

56. Okitsu, K. Sonochemical synthesis of metal nanoparticles. In *Theoretical and Experimental Sonochemistry Involving Inorganic Systems*; Pankaj, A.M., Ed.; Springer: Dordrecht, The Netherlands, 2011; pp. 131–150.

57. Anandan, S.; Ashokkumar, M. Sonochemical preparation of monometallic, bimetallic and metal-loaded semiconductor nanoparticles. In *Theoretical and Experimental Sonochemistry Involving Inorganic Systems*; Pankaj, A.M., Ed.; Springer: Dordrecht, The Netherlands, 2011; pp. 151–169.

58. Okitsu, K. Generation of size, structure, and shape-controlled metal nanoparticles using cavitation. In *Cavitation: A Novel Energy-Efficient Technique for the Generation of Nanomaterials*; Manickam, S., Ashokkumar, M., Eds.; Pan Stanford: Singapore, 2014; pp. 29–54.

59. Anandan, S.; Ashokkumar, M. Sonochemical synthesis of noble monometallic and bimetallic nanoparticles for catalytic applications. In *Cavitation: A Novel Energy-Efficient Technique for the Generation of Nanomaterials*; Manickam, S., Ashokkumar, M., Eds.; Pan Stanford: Singapore, 2014; pp. 55–88.

60. Okitsu, K.; Ashokkumar, M.; Grieser, F. Sonochemical synthesis of gold nanoparticles: Effects of ultrasound frequency. *J. Phys. Chem. B* **2005**, *109*, 20673–20675. [CrossRef] [PubMed]

61. Okitsu, K.; Yue, A.; Tanabe, S.; Matsumoto, H. Sonochemical preparation and catalytic behavior of highly dispersed palladium nanoparticles on alumina. *Chem. Mater.* **2000**, *12*, 3006–3011. [CrossRef]

62. Dhas, N.A.; Gedanken, A. Sonochemical preparation and properties of nanostructured palladium metallic clusters. *J. Mater. Chem.* **1998**, *8*, 445–450. [CrossRef]

63. Qiu, L.; Pol, V.G.; Calderon-Moreno, J.; Gedanken, A. Synthesis of tin nanorods via a sonochemical method combined with a polyol process. *Ultrason. Sonochem.* **2005**, *12*, 243–247. [CrossRef]

64. Gedanken, A. Using sonochemistry for the fabrication of nanomaterials. *Ultrason. Sonochem.* **2004**, *11*, 47–55. [CrossRef] [PubMed]

65. Mizukoshi, Y.; Takagi, E.; Okuno, H.; Oshima, R.; Maeda, Y.; Nagata, Y. Preparation of platinum nanoparticles by sonochemical reduction of the Pt(IV) ions: Role of surfactants. *Ultrason. Sonochem.* **2001**, *8*, 1–6. [CrossRef] [PubMed]

66. Pollet, B.G. The use of ultrasound for the fabrication of fuel cell materials. *Int. J. Hydrog. Energy* **2010**, *35*, 11986–12004. [CrossRef]

67. Dhas, N.A.; Raj, C.P.; Gedanken, A. Synthesis, characterization, and properties of metallic copper nanoparticles. *Chem. Mater.* **1998**, *10*, 1446–1452. [CrossRef]

68. Caruso, R.A.; Ashokkumar, M.; Grieser, F. Sonochemical formation of gold sols. *Langmuir* **2002**, *18*, 7831–7836. [CrossRef]

69. Sakai, T.; Enomoto, H.; Torigoe, K.; Sakai, H.; Abe, M. Surfactant- and reducer-free synthesis of gold nanoparticles in aqueous solutions. *Colloids Surf. A Physicochem. Eng. Asp.* **2009**, *347*, 18–26. [CrossRef]

70. Sakai, T.; Enomoto, H.; Sakai, H.; Abe, M. Hydrogen-assisted fabrication of spherical gold nanoparticles through sonochemical reduction of tetrachloride gold(III) ions in water. *Ultrason. Sonochem.* **2014**, *21*, 946–950. [CrossRef] [PubMed]

71. Hansen, H.E.; Seland, F.; Sunde, S.; Burheim, O.S.; Pollet, B.G. Frequency controlled agglomeration of Pt-nanoparticles in sonochemical synthesis. *Ultrason. Sonochem.* **2022**, *85*, 105991. [CrossRef]

72. Okitsu, K.; Semboshi, S. Synthesis of Au nanorods via autocatalytic growth of Au seeds formed by sonochemical reduction of Au(I): Relation between formation rate and characteristic of Au nanorods. *Ultrason. Sonochem.* **2020**, *69*, 105229. [CrossRef] [PubMed]

73. Hansen, H.E.; Fakhri, D.Ø.; Seland, F.; Sunde, S.; Burheim, O.S.; Pollet, B.G. Sonochemical synthesis of Cu@Pt bimetallic nanoparticles. *Molecules* **2022**, *27*, 5281. [CrossRef]

74. Meichtry, J.M.; Cancelada, L.; Destaillats, H.; Litter, M.I. Effect of different gases on the sonochemical Cr(VI) reduction in the presence of citric acid. *Chemosphere* **2020**, *260*, 127211. [CrossRef]

75. Hoinkis, N.; Litter, M.I. Mechanisms of sonochemical transformation of nitrate and nitrite under different conditions: Influence of additives and pH. *Ind. Eng. Chem. Res.* **2022**, *61*, 16408–16417. [CrossRef]

76. Okitsu, K.; Kurisaka, I.; Nanzai, B.; Takenaka, N.; Bandow, H. Mechanism for sonochemical reduction of Au(III) in aqueous butanol solution under Ar based on the analysis of gaseous and water-soluble products. *Ultrason. Sonochem.* **2020**, *69*, 105241. [CrossRef]

77. Yasui, K. Effect of volatile solutes on sonoluminescence. *J. Chem. Phys.* **2002**, *116*, 2945–2954. [CrossRef]

78. Kamali, M.; Davarazar, M.; Aminabhavi, T.M. Single precursor sonochemical synthesis of mesoporous hexagonal-shape zero-valent copper for effective nitrate reduction. *Chem. Eng. J.* **2020**, *384*, 123359. [CrossRef]

79. Saleh, N.M.; Aziz, A.A. Simulation of surface plasmon resonance on different size of a single gold nanoparticle. *J. Phys. Conf. Ser.* **2018**, *1083*, 012041. [CrossRef]

80. Yasui, K. Single-bubble sonoluminescence from hydrogen. *J. Chem. Phys.* **1999**, *111*, 5384–5389. [CrossRef]

81. Gutierrez, M.; Henglein, A.; Dohrmann, J.K. H atom reactions in the sonolysis of aqueous solutions. *J. Phys. Chem.* **1987**, *91*, 6687–6690. [CrossRef]

82. Yasui, K. Unsolved problems in acoustic cavitation. In *Handbook of Ultrasonics and Sonochemistry*; Ashokkumar, M., Cavalieri, F., Chemat, F., Okitsu, K., Sambandam, A., Yasui, K., Zisu, B., Eds.; Springer: Singapore, 2016; Volume 1, pp. 259–292.

83. Yasui, K.; Tuziuti, T.; Kanematsu, W. Mechanism of OH radical production from ozone bubbles in water after stopping cavitation. *Ultrason. Sonochem.* **2019**, *58*, 104707. [CrossRef]

84. Yasuda, K.; Sato, T.; Asakura, Y. Size-controlled synthesis of gold nanoparticles by ultrafine bubbles and pulsed ultrasound. *Chem. Eng. Sci.* **2020**, *217*, 115527. [CrossRef]

85. Terasaka, K. Introduction to experiments. In *Ultrafine Bubbles*; Terasaka, K., Yasui, K., Kanematsu, W., Aya, N., Eds.; Jenny Stanford: Singapore, 2022; pp. 17–72.

86. Wang, W.; Fan, W.; Huo, M.; Zhao, H.; Lu, Y. Hydroxyl radical generation and contaminant removal from water by the collapse of microbubbles under different hydrochemical conditions. *Water Air Soil Pollut.* **2018**, *229*, 86. [CrossRef]

87. Takahashi, M. Nanobubbles: An introduction. In *Micro- and Nanobubbles*; Tsuge, H., Ed.; Pan Stanford: Singapore, 2014; pp. 307–315.

88. Kanematsu, W.; Tuziuti, T.; Yasui, K. The influence of storage conditions and container materials on the long term stability of bulk nanobubbles—Consideration from a perspective of interactions between bubbles and surroundings. *Chem. Eng. Sci.* **2020**, *219*, 115594. [CrossRef]

89. Yasui, K.; Tuziuti, T.; Kanematsu, W. Interaction of bulk nanobubbles (ultrafine bubbles) with a solid surface. *Langmuir* **2021**, *37*, 1674–1681. [CrossRef]

90. Yasui, K.; Tuziuti, T.; Kanematsu, W.; Kato, K. Dynamic equilibrium model for a bulk nanobubble and a microbubble partly covered with hydrophobic material. *Langmuir* **2016**, *32*, 11101–11110. [CrossRef]

91. Yasui, K.; Tuziuti, T.; Kanematsu, W. Mysteries of bulk nanobubbles (ultrafine bubbles); stability and radical formation. *Ultrason. Sonochem.* **2018**, *48*, 259–266. [CrossRef]

92. Sugano, K.; Miyoshi, Y.; Inazato, S. Study of ultrafine bubble stabilization by organic material adhesion. *Jpn. J. Multiph. Flow* **2017**, *31*, 299–306. [CrossRef]

93. Sugano, K.; Miyoshi, Y.; Inazato, S. Study of ultrafine bubbles stabilization by organic material adhesion. In *Ultrafine Bubbles*; Terasaka, K., Yasui, K., Kanematsu, W., Aya, N., Eds.; Jenny Stanford: Singapore, 2022; pp. 155–177.

94. Yasui, K. Theory of ultrafine bubbles. In *Ultrafine Bubbles*; Terasaka, K., Yasui, K., Kanematsu, W., Aya, N., Eds.; Jenny Stanford: Singapore, 2022; pp. 109–153.

95. Yasui, K. Critical roles of impurities and imperfections in various phases of materials. *Materials* **2023**, *16*, 1612. [CrossRef] [PubMed]

96. Yasui, K. On some aspects of nanobubble-containing systems. *Nanomaterials* **2022**, *12*, 2175. [CrossRef] [PubMed]

97. Asakura, Y. Experimental methods in sonochemistry. In *Sonochemistry and the Acoustic Bubble*; Grieser, F., Choi, P.-K., Enomoto, N., Harada, H., Okitsu, K., Yasui, K., Eds.; Elsevier: Amsterdam, The Netherlands, 2015; pp. 119–150.

98. Sonoda, A. Real UFB sample measurements: A few cases. In *Ultrafine Bubbles*; Terasaka, K., Yasui, K., Kanematsu, W., Aya, N., Eds.; Jenny Stanford: Singapore, 2022; pp. 87–108.

99. Tuziuti, T.; Yasui, K.; Kanematsu, W. Decrease in the surface tension of nanobubble dispersion in water: Results of surface excess of bulk nanobubbles at interfaces. *Langmuir* **2023**, *39*, 5771–5778. [CrossRef] [PubMed]

100. Kamath, V.; Prosperetti, A.; Egolfopoulos, F.N. A theoretical study of sonoluminescence. *J. Acoust. Soc. Am.* **1993**, *94*, 248–260. [CrossRef]

101. Storey, B.D.; Szeri, A.J. Water vapour, sonoluminescence and sonochemistry. *Proc. R. Soc. A* **2000**, *456*, 1685–1709. [CrossRef]

102. Storey, B.D.; Szeri, A.J. A reduced model of cavitation physics for use in sonochemistry. *Proc. R. Soc. A* **2001**, *457*, 1685–1700. [CrossRef]

103. An, Y. Mechanism of single-bubble sonoluminescence. *Phys. Rev. E* **2006**, *74*, 026304. [CrossRef]

104. Kalmár, C.; Klapcsik, K.; Hegedűs, F. Relationship between the radial dynamics and the chemical production of a harmonically driven spherical bubble. *Ultrason. Sonochem.* **2020**, *64*, 104989. [CrossRef]

105. Kalmár, C.; Turányi, T.; Zsély, I.G.; Papp, M.; Hegedűs, F. The importance of chemical mechanisms in sonochemical modelling. *Ultrason. Sonochem.* **2022**, *83*, 105925. [CrossRef]

106. Merouani, S.; Hamdaoui, O.; Rezgui, Y.; Guemini, M. Sensitivity of free radicals production in acoustically driven bubble to the ultrasonic frequency and nature of dissolved gases. *Ultrason. Sonochem.* **2015**, *22*, 41–50. [CrossRef]

107. Kerboua, K.; Merouani, S.; Hamdaoui, O.; Alghyamah, A.; Islam, M.H.; Hansen, H.E.; Pollet, B.G. How do dissolved gases affect the sonochemical process of hydrogen production? an overview of thermodynamic and mechanistic effects–on the "hot spot theory". *Ultrason. Sonochem.* **2021**, *72*, 105422. [CrossRef]

108. Hauke, G.; Fuster, D.; Dopazo, C. Dynamics of a single cavitating and reacting bubble. *Phys. Rev. E* **2007**, *75*, 066310. [CrossRef]

109. Yuan, L. Sonochemical effects on single-bubble sonoluminescence. *Phys. Rev. E* **2005**, *72*, 046309. [CrossRef]

110. Gong, C.; Hart, D.P. Ultrasound induced cavitation and sonochemical yields. *J. Acoust. Soc. Am.* **1998**, *104*, 2675–2682. [CrossRef]

111. Yasui, K. Numerical simulations for sonochemistry. *Ultrason. Sonochem.* **2021**, *78*, 105728. [CrossRef] [PubMed]

112. Yasui, K. Variation of liquid temperature at bubble wall near the sonoluminescence threshold. *J. Phys. Soc. Jpn.* **1996**, *65*, 2830–2840. [CrossRef]

113. Yasui, K. Effect of liquid temperature on sonoluminescence. *Phys. Rev. E* **2001**, *64*, 016310. [CrossRef] [PubMed]

114. Yasui, K.; Tuziuti, T.; Iida, Y.; Mitome, H. Theoretical study of the ambient-pressure dependence of sonochemical reactions. *J. Chem. Phys.* **2003**, *119*, 346–356. [CrossRef]

115. Yasui, K. Effect of non-equilibrium evaporation and condensation on bubble dynamics near the sonoluminescence threshold. *Ultrasonics* **1998**, *36*, 575–580. [CrossRef]

116. Yasui, K.; Tuziuti, T.; Iida, Y. Optimum bubble temperature for the sonochemical production of oxidants. *Ultrasonics* **2004**, *42*, 579–584. [CrossRef] [PubMed]

117. Yasui, K. Segregation of vapor and gas in a sonoluminescing bubble. *Ultrasonics* **2002**, *40*, 643–647. [CrossRef]

118. Baulch, D.L.; Drysdale, D.D.; Horne, D.G.; Lloyd, A.C. Homogeneous Gas Phase Reactions of the H_2-O_2 System. In *Evaluated Kinetic Data for High Temperature Reactions*; Butterworths: London, UK, 1972; Volume 1.

119. Baulch, D.L.; Drysdale, D.D.; Horne, D.G.; Lloyd, A.C. Homogeneous Gas Phase Reactions of the H_2-N_2-O_2 System. In *Evaluated Kinetic Data for High Temperature Reactions*; Butterworths: London, UK, 1973; Volume 2.

120. Baulch, D.L.; Drysdale, D.D.; Duxbury, J.; Grant, S.J. Homogeneous Gas Phase Reactions of the O_2-O_3 Systems, the CO-O_2-H_2 System, and of Sulphur-containing Species. In *Evaluated Kinetic Data for High Temperature Reactions*; Butterworths: London, UK, 1976; Volume 3.

121. Matula, T.J.; Cordry, S.M.; Roy, R.A.; Crum, L.A. Bjerknes force and bubble levitation under single-bubble sonoluminescence conditions. *J. Acoust. Soc. Am.* **1997**, *102*, 1522–1527. [CrossRef]

122. Barber, B.P.; Hiller, R.A.; Löfstedt, R.; Putterman, S.J.; Weninger, K.R. Defining the unknowns of sonoluminescence. *Phys. Rep.* **1997**, *281*, 65–143. [CrossRef]

123. Barber, B.P.; Putterman, S.J. Observation of synchronous picosecond sonoluminescence. *Nature* **1991**, *352*, 318–320. [CrossRef]
124. Didenko, Y.T.; Suslick, K.S. The energy efficiency of formation of photons, radicals and ions during single-bubble cavitation. *Nature* **2002**, *418*, 394–397. [CrossRef] [PubMed]
125. Lohse, D.; Brenner, M.P.; Dupont, T.F.; Hilgenfeldt, S.; Johnston, B. Sonoluminescing air bubbles rectify argon. *Phys. Rev. Lett.* **1997**, *78*, 1359–1362. [CrossRef]
126. Matula, T.J.; Crum, L.A. Evidence for gas exchange in single-bubble sonoluminescence. *Phys. Rev. Lett.* **1998**, *80*, 865–868. [CrossRef]
127. Yasui, K. Merits and demerits of ODE modeling of physicochemical systems for numerical simulations. *Molecules* **2022**, *27*, 5860. [CrossRef]
128. Armstrong, D.A.; Huie, R.E.; Koppenol, W.H.; Lymar, S.V.; Merényi, G.; Neta, P.; Ruscic, B.; Stanbury, D.M.; Steenken, S.; Wardman, P. Standard electrode potentials involving radicals in aqueous solution: Inorganic radicals (IUPAC technical report). *Pure Appl. Chem.* **2015**, *87*, 1139–1150. [CrossRef]
129. Bard, A.J.; Parsons, R.; Jordan, J. (Eds.) *Standard Potentials in Aqueous Solutions*; Marcel Dekker: New York, NY, USA, 1985.
130. Rao, P.S.; Hayon, E. Redox potentials of free radicals. I. simple organic radicals. *J. Am. Chem. Soc.* **1974**, *96*, 1287–1294. [CrossRef]
131. Makino, K.; Mossoba, M.M.; Riesz, P. Chemical effects of ultrasound on aqueous solutions. Formation of hydroxyl radicals and hydrogen atoms. *J. Phys. Chem.* **1983**, *87*, 1369–1377. [CrossRef]
132. Carmichael, A.J.; Mossoba, M.M.; Riesz, P.; Christman, C.L. Free radical production in aqueous solutions exposed to simulated ultrasonic diagnostic conditions. *IEEE Trans. Ultrason. Ferroelectr. Freq. Control* **1986**, *33*, 148–155. [CrossRef] [PubMed]
133. Riesz, P.; Berdahl, D.; Christman, C.L. Free radical generation by ultrasound in aqueous and nonaqueous solutions. *Environ. Health Perspect.* **1985**, *64*, 233–252. [CrossRef]
134. Fischer, C.H.; Hart, E.J.; Henglein, A. H/D isotope exchange in the D_2–H_2O system under the influence of ultrasound. *J. Phys. Chem.* **1986**, *90*, 222–224. [CrossRef]
135. Fischer, C.H.; Hart, E.J.; Henglein, A. H/D isotope exchange in the HD–H_2O system under the influence of ultrasound. *J. Phys. Chem.* **1986**, *90*, 3059–3060. [CrossRef]
136. Hart, E.J.; Henglein, A. Sonolytic decomposition of nitrous oxide in aqueous solution. *J. Phys. Chem.* **1986**, *90*, 5992–5995. [CrossRef]
137. Kerboua, K.; Hamdaoui, O.; Islam, M.H.; Alghyamah, A.; Hansen, H.E.; Pollet, B.G. Low carbon ultrasonic production of alternate fuel: Operational and mechanistic concerns of the sonochemical process of hydrogen generation under various scenarios. *Int. J. Hydrog. Energy* **2021**, *46*, 26770–26787. [CrossRef]
138. Rashwan, S.S.; Dincer, I.; Mohany, A. An investigation of ultrasonic based hydrogen production. *Energy* **2020**, *205*, 118006. [CrossRef]
139. Rashwan, S.S.; Dincer, I.; Mohany, A. A unique study on the effect of dissolved gases and bubble temperatures on the ultrasonic hydrogen (sonohydrogen) production. *Int. J. Hydrog. Energy* **2020**, *45*, 20808–20819. [CrossRef]
140. Rashwan, S.S.; Dincer, I.; Mohany, A. A review on the importance of operating conditions and process parameters in sonic hydrogen production. *Int. J. Hydrog. Energy* **2021**, *46*, 28418–28434. [CrossRef]
141. Dehane, A.; Merouani, S.; Hamdaoui, O.; Yasui, K.; Ashokkumar, M. A hydrogen-based technique for determining the number density of acoustic microreactors (actives bubbles) in sonicated solutions. *Int. J. Hydrog. Energy* **2023**, *48*, 13430–13441. [CrossRef]
142. Mead, E.L.; Sutherland, R.G.; Verrall, R.E. The effect of ultrasound on water in the presence of dissolved gases. *Can. J. Chem.* **1976**, *54*, 1114–1120. [CrossRef]
143. Lide, D.R. (Ed.) *CRC Handbook of Chemistry and Physics*, 75th ed.; CRC Press: Boca Raton, FL, USA, 1994.
144. Kwedi-Nsah, L.-M.; Kobayashi, T. Sonochemical nitrogen fixation for the generation of NO_2^- and NO_3^- ions under high-powered ultrasound in aqueous medium. *Ultrason. Sonochem.* **2020**, *66*, 105051. [CrossRef] [PubMed]
145. Son, Y.; Choi, J. Effects of gas saturation and sparging on sonochemical oxidation activity in open and closed systems, part II: NO_2^-/NO_3^- generation and a brief critical review. *Ultrason. Sonochem.* **2023**, *92*, 106250. [CrossRef]
146. Yang, Y.; Cho, Y.I.; Fridman, R.S. *Plasma Discharge in Liquid*; CRC Press: Boca Raton, FL, USA, 2012.
147. Okitsu, K.; Iwatani, M.; Nanzai, B.; Nishimura, R.; Maeda, Y. Sonochemical reduction of permanganate to manganese dioxide: The effects of H_2O_2 formed in the sonolysis of water on the rates of reduction. *Ultrason. Sonochem.* **2009**, *16*, 387–391. [CrossRef]
148. Bielski, B.H.J.; Cabelli, D.E.; Arudi, R.L.; Ross, A.B. Reactivity of HO_2/O^-_2 radicals in aqueous solution. *J. Phys. Chem. Ref. Data* **1985**, *14*, 1041–1100. [CrossRef]
149. Kondo, T.; Mišík, V.; Riesz, P. Sonochemistry of cytochrome c. evidence for superoxide formation by ultrasound in argon-saturated aqueous solution. *Ultrason. Sonochem.* **1996**, *3*, S193–S199. [CrossRef]
150. Morrissey, J.M.; Taylor, K.D.; Gilman, S.D. Ultrasound-mediated release of iron from ferritin. *Ultrasound Med. Biol.* **2003**, *29*, 1799–1803. [CrossRef]
151. Castellanos, M.M.; Reyman, D.; Sieiro, C.; Calle, P. ESR-spin trapping study on the sonochemistry of liquids in the presence of oxygen. Evidence for the superoxide radical anion formation. *Ultrason. Sonochem.* **2001**, *8*, 17–22. [CrossRef]
152. Matheson, M.S.; Rabani, J. Pulse radiolysis of aqueous hydrogen solutions. I. Rate constants for reaction of e_{aq}^- with itself and other transients. II. The interconvertibility of e_{aq}^- and H^1. *J. Phys. Chem.* **1965**, *69*, 1324–1335. [CrossRef]
153. Flannigan, D.J.; Suslick, K.S. Plasma formation and temperature measurement during single-bubble cavitation. *Nature* **2005**, *434*, 52–55. [CrossRef] [PubMed]

154. Kappus, B.; Bataller, A.; Putterman, S.J. Energy balance for a sonoluminescence bubble yields a measure of ionization potential lowering. *Phys. Rev. Lett.* **2013**, *111*, 234301. [CrossRef]
155. Yasui, K.; Kato, K. Bubble dynamics and sonoluminescence from helium or xenon in mercury and water. *Phys. Rev. E* **2012**, *86*, 036320. [CrossRef] [PubMed]
156. Sharipov, G.L.; Gareev, B.M.; Vasilyuk, K.S.; Galimov, D.I.; Abdrakhmanov, A.M. New sonochemiluminescence involving solvated electron in Ce(III)/Ce(IV) solutions. *Ultrason. Sonochem.* **2021**, *70*, 105313. [CrossRef]
157. Mišík, V.; Riesz, P. Effect of Cd^{2+} on the $^{\bullet}$H atom yield in the sonolysis of water. Evidence against the formation of hydrated electrons. *J. Phys. Chem. A* **1997**, *101*, 1441–1444. [CrossRef]
158. Yasui, K. Temperature in multibubble sonoluminescence. *J. Chem. Phys.* **2001**, *115*, 2893–2896. [CrossRef]
159. Yasui, K.; Tuziuti, T.; Iida, Y. Dependence of the characteristics of bubbles on types of sonochemical reactors. *Ultrason. Sonochem.* **2005**, *12*, 43–51. [CrossRef]
160. Yasui, K.; Kozuka, T.; Tuziuti, T.; Towata, A.; Iida, Y.; King, J.; Macey, P. FEM calculation of an acoustic field in a sonochemical reactor. *Ultrason. Sonochem.* **2007**, *14*, 605–614. [CrossRef]
161. Yasui, K. Influence of ultrasonic frequency on multibubble sonoluminescence. *J. Acoust. Soc. Am.* **2002**, *112*, 1405–1413. [CrossRef]
162. Mettin, R.; Luther, S.; Ohl, C.-D.; Lauterborn, W. Acoustic cavitation structures and simulations by a particle model. *Ultrason. Sonochem.* **1999**, *6*, 25–29. [CrossRef]
163. Lauterborn, W.; Kurz, T.; Mettin, R.; Ohl, C.D. Experimental and theoretical bubble dynamics. *Adv. Chem. Phys.* **1999**, *110*, 295–380. [CrossRef]
164. Yasui, K.; Iida, Y.; Tuziuti, T.; Kozuka, T.; Towata, A. Strongly interacting bubbles under an ultrasonic horn. *Phys. Rev. E* **2008**, *77*, 016609. [CrossRef]
165. Stricker, L.; Dollet, B.; Rivas, D.F.; Lohse, D. Interacting bubble clouds and their sonochemical production. *J. Acoust. Soc. Am.* **2013**, *134*, 1854–1862. [CrossRef] [PubMed]
166. Dehane, A.; Merouani, S.; Chibani, A.; Hamdaoui, O.; Ashokkumar, M. Sonochemical and sono-assisted reduction of carbon dioxide: A critical review. *Chem. Eng. Process.* **2022**, *179*, 109075. [CrossRef]
167. Yasuda, K. Sonochemical green technology using active bubbles: Degradation of organic substances in water. *Curr. Opin. Green Sustain. Chem.* **2021**, *27*, 100411. [CrossRef]
168. Pham, T.M.H.; Vu, M.T.; Cong, T.D.; Nguyen, N.S.; Doan, T.A.; Truong, T.T.; Nguyen, T.H. Green sonochemical process for preparation of polyethylene glycol–Fe_3O_4/ZnO magnetic nanocomposite using rambutan peel extract as photocatalyst, for removal of methylene blue in solution. *Bull. Mater. Sci.* **2022**, *45*, 13. [CrossRef]
169. Chen, T.-W.; Chinnapaiyan, S.; Chen, S.-M.; Mahmoud, A.H.; Elshikh, M.S.; Ebaid, H.; Yassin, M.T. Facile sonochemical synthesis of rutile-type titanium dioxide microspheres decorated graphene oxide composite for efficient electrochemical sensor. *Ultrason. Sonochem.* **2020**, *62*, 104872. [CrossRef]
170. Zheng, H.; Zheng, Y.; Zhu, J. Recent developments in hydrodynamic cavitation reactors: Cavitation mechanism, reactor design, and applications. *Engineering* **2022**, *19*, 180–198. [CrossRef]
171. Talabazar, F.R.; Aghdam, A.S.; Jafarpour, M.; Grishenkov, D.; Koşar, A.; Ghorbani, M. Chemical effects in "hydrodynamic cavitation on a chip": The role of cavitating flow patterns. *Chem. Eng. J.* **2022**, *445*, 136734. [CrossRef]
172. Zhang, Z.; Lu, J.; Lv, B.; Liu, W.; Shen, S.; Wang, D.; Ji, J. Chemical effects induced by gas-liquid jet flow. *React. Chem. Eng.* **2022**, *7*, 566–569. [CrossRef]
173. Podbevšek, D.; Ledoux, G.; Dular, M. Investigation of hydrodynamic cavitation induced reactive oxygen species production in microchannels via chemiluminescent luminol oxidation reactions. *Water Res.* **2022**, *220*, 118628. [CrossRef] [PubMed]
174. Sun, X.; Liu, J.; Ji, L.; Wang, G.; Zhao, S.; Yoon, J.Y.; Chen, S. A review on hydrodynamic cavitation disinfection: The current state of knowledge. *Sci. Total Environ.* **2020**, *737*, 139606. [CrossRef] [PubMed]